# RSC Advances



This is an *Accepted Manuscript*, which has been through the Royal Society of Chemistry peer review process and has been accepted for publication.

Accepted Manuscripts are published online shortly after acceptance, before technical editing, formatting and proof reading. Using this free service, authors can make their results available to the community, in citable form, before we publish the edited article. This Accepted Manuscript will be replaced by the edited, formatted and paginated article as soon as this is available.

You can find more information about *Accepted Manuscripts* in the **Information for Authors**.

Please note that technical editing may introduce minor changes to the text and/or graphics, which may alter content. The journal's standard <u>Terms & Conditions</u> and the <u>Ethical guidelines</u> still apply. In no event shall the Royal Society of Chemistry be held responsible for any errors or omissions in this *Accepted Manuscript* or any consequences arising from the use of any information it contains.



## Pyridyl vs bipyridyl anchoring groups of porphyrin sensitizers for dye sensitized solar cells

Panagiotis A. Angaridis, $^{\dagger}$  Eleftherios Ferentinos, $^{\S}$  Georgios Charalambidis, $^{\S}$  Kalliopi Ladomenou, $^{\S}$  Vasilis Nikolaou, $^{\S}$ S. Biswas $^{\sharp}$ , Ganesh D. Sharma $^{*,\sharp}$  and Athanassios G. Coutsolelos $^{*,\S}$ 

# Molecular Electronics and Optoelectronics Device Research Laboratory

Department of Physics, LNMIIT, Jamdoli, Jaipur (Raj.) 302301, India

keywords: Porphyrin, anchoring groups, pyridine, bipyridine, DSSC

<sup>&</sup>lt;sup>†</sup> Department of Chemistry, Aristotle University of Thessaloniki, Thessaloniki 54124, Greece

<sup>§</sup> Department of Chemistry, University of Crete, Laboratory of Bioinorganic Chemistry, Voutes Campus, P.O. Box 2208, 71003, Heraklion, Crete, Greece

**ABSTRACT:** The synthesis of two porphyrins with donor- $\pi$ -acceptor (D- $\pi$ -A) molecular architecture is described, namely Znpor-py (3a) and Znpor-bpy (3b), which consist of a 4tert-butyl-phenyl group as donor and either a pyridine or a bipyridine group as acceptor at opposite positions of the porphyrin macrocycle. Photophysical and electrochemical properties of the two compounds, as well as theoretical DFT calculation results suggest that the two porphyrins have the potential to act as sensitizers in dye-sensitized solar cells (DSSCs). Both dyes contain N(pyridyl) atoms able to act as anchors onto the acid sites of TiO<sub>2</sub>. Znpor-py (3a) sensitized solar cell was found to exhibit power conversion efficiency (PCE) of 3.57%, while the corresponding Znpor-bpy (3b)-functionalized solar cell showed a higher PCE of 5.08%. The enhanced short circuit current  $J_{\rm sc}$  and open circuit voltage  $V_{\rm oc}$  parameters are the main factors responsible for the improved photovoltaic performance of the latter solar cell. These are attributed to its faster charge injection into the TiO<sub>2</sub> photoanode and its reduced charge recombination at the electrode/electrolyte interface, which result from the stronger binding and coordination geometry of the bipyridine anchoring group on TiO<sub>2</sub>. Electrochemical impedance spectra (EIS) of the two solar cells further support these assumptions, revealing a higher charge recombination resistance  $R_{rec}$  and a longer electron lifetime  $\tau_e$  for the Znpor-bpy (3b) sensitized solar cell.

### INTRODUCTION

Dye sensitized solar cells (DSSCs), since their first report in 1991,<sup>1</sup> have attracted considerable research interest, owing to their potential use in solar-into-electrical energy conversion devices that exhibit high power conversion efficiencies (PCE),and low cost of fabrication.<sup>2-7</sup> Photosensitizers are key components of DSSCs, which are responsible for absorbing photons and injecting electrons, upon their excitation, into the TiO<sub>2</sub> conduction band at the anode electrode of the devices.<sup>8-10</sup> Thus, the development of new efficient sensitizers has become a very attractive and challenging field of today's research. Among the most efficient DSSC sensitizers are ruthenium-polypyridyl complexes, which have allowed the fabrication of DSSCs with PCE values of 11%.<sup>11-13</sup> However, the limited resources and the high cost of ruthenium metal substantially hinder their practical application.

Over the last decade, many efforts have been devoted to the design of new, low-cost, noble metal-free DSSC sensitizers.<sup>2, 14, 15</sup> The basic design strategy for efficient dyes of this type is the synthesis of molecules with a donor-π-acceptor (D-π-A) or "push-pull" molecular architecture, which, in some cases, resulted in PCE values of 10%.<sup>16-19</sup> Porphyrins constitute a particular type of noble metal-free dyes considered to be a very promising class of DSSC sensitizers.<sup>20-30</sup> This is due to their unique properties, which include efficient solar energy absorption in the visible region of electromagnetic spectrum with high molar extinction coefficients, suitable highest occupied molecular orbital (HOMO) and lowest unoccupied molecular orbital (LUMO) energy levels, and ability to control their physicochemical properties through appropriate synthetic modification. Indeed, porphyrin based sensitizers with "push-pull" molecular architectures have resulted in DSSCs that exhibit higher than 10%PCE values,<sup>31-37</sup> with the most efficient porphyrin dyes reaching the impressive PCE values of 12-13%.<sup>38-40</sup>

In most of these noble metal-free D- $\pi$ -A sensitizers, carboxylic acids and cyanoacrylic acid have commonly been used as acceptor and anchoring groups for the attachment of the dye onto the TiO<sub>2</sub> surface of the anode electrode. Among them, cyanoacrylic acid has been proved to be the most effective, since it red shifts and broadens the absorption spectra of the corresponding dyes resulting in enhanced electron injection efficiencies. However, the use of cyanoacrylic acid as binding unit also results in fast degradation of the dyes on the TiO<sub>2</sub> surface, affecting the device long-term stability.<sup>41</sup> Moreover, it can undergo *trans*-to-*cis*-photo isomerization, a process that competes with electron injection and has a harmful effect on the cell performance.<sup>42</sup> Recently, a tropolone group has been employed for the first time as an anchoring group for dye-sensitized solar cells, enhancing the binding ability with respect to its carboxylic analogue porphyrin.<sup>43</sup>

Other electron accepting units that have been recently examined as anchoring groups in DSSC sensitizers<sup>44</sup> include pyridine<sup>45-48</sup> and pyridinium groups.<sup>49</sup> The coordinate bond of the N-atom of the pyridyl group to the Lewis acid sites of TiO<sub>2</sub> provides good electron communication between them, leading to very efficient electron injection. In 2013, Wang and coworkers first reported DSSCs sensitized by D- $\pi$ -A porphyrin dyes with pyridyl anchoring groups, which resulted in PCE values of ~4.0%.<sup>50</sup> Furthermore, Sun and coworkers employed *N*-(carboxymethyl) pyridinium as electron-withdrawing anchoring group for a series of hemicyanine dyes, which showed PCE values higher than their cyanoacrylic acid counterparts (~7.0%). Moreover, Grätzel and coworkers have employed porphyrin sensitizers bearing pyridyl anchoring groups resulting in DSSCs with PCE values of 8.5% and impressing long-term stability.<sup>51</sup>

Our research group has also reported the use of simple porphyrin sensitizers with pyridyl anchoring groups for the fabrication of DSSCs, which reached a maximum PCE value of 3.9%.<sup>52</sup> In a more recent report, we synthesized two tetra-aryl substituted, "spider-shaped"

zinc-metallated porphyrins, bearing four oligo (*p*-phenylenevinylene) pyridyl groups with long dodecyloxy chains on the phenyl groups, as sensitizers for the fabrication of DSSCs achieving a maximum PCE of 5.12%.<sup>53</sup> Continuing our efforts towards this direction, we describe herein the synthesis, and optical, electrochemical, and photovoltaic properties of two simple "push-pull" porphyrins bearing pyridyl (py) and bipyridyl (bpy) acceptor-anchoring groups, namely the compounds Znpor-py (**3a**) and Znpor-bpy (**3b**)(Scheme 1). Moreover, we compare the effect of pyridyl and bipyridyl anchoring groups on the photovoltaic performance of the corresponding DSSCs.

### **EXPERIMENTAL SECTION**

**Materials and techniques**: All manipulations were carried out using standard Schlenk techniques under nitrogen atmosphere. Pyridine-4-carbaldehyde, 4-*tert*-butyl-benzaldehyde, BF<sub>3</sub>·OEt<sub>2</sub>, 2,3-dichloro-5,6-dicyano-1,4-benzoquinone (DDQ), Et<sub>3</sub>N, Zn(CH<sub>3</sub>COO)<sub>2</sub>·2H<sub>2</sub>O, N-bromo succinamide (NBS) and other chemicals and solvents were purchased from usual commercial sources and used as received, unless otherwise stated. Dipyrromethane<sup>54</sup> and bipyridine-4-carbaldehyde<sup>55, 56</sup> were prepared according to literature procedures.

**5-(4-***tert*-**butyl-phenyl)-15-(4-pyridyl)-porphyrin(1a):** To a degassed CH<sub>2</sub>Cl<sub>2</sub>/MeOH mixture (90/10 v/v, 600 mL) dipyrromethane (0.74 g, 5.06 mmol), pyridine-4-carbaldehyde (0.24 mL, 2.53 mmol) and 4-*tert*-butyl-benzaldehyde (0.42 mL, 2.53 mmol) were successively added under nitrogen in the dark. After 20-min nitrogen bubbling, BF<sub>3</sub>·OEt<sub>2</sub> (1.74 mL, 14.1 mmol) was slowly added in three portions, and the mixture was stirred for 2 days. Then DDQ (1.724 g, 7.59 mmol) was added and the mixture was further stirred for 20 h before addition of Et<sub>3</sub>N (2.1 mL). After 30 min of stirring, the mixture was filtered through silica pad and the filtrate was evaporated to dryness. The crude product was subjected to silica gel column chromatography using CH<sub>2</sub>Cl<sub>2</sub> as eluent, from which collecting the second

red band isolated the desired asymmetric trans-AB porphyrin. After evaporation of the solvent, the product was further purified by a short alumina column chromatography with CH<sub>2</sub>Cl<sub>2</sub> as eluent. The solvent was removed and, after washing with *n*-hexane (50 mL), porphyrin **1a** was isolated as red-brown powder (0.18 g, 13%). mp >300 °C. <sup>1</sup>H NMR (300 MHz, CDCl<sub>3</sub> + 1% Et<sub>3</sub>N):  $\delta$  10.34 (s, 2H), 9.42 (m, 4H), 9.16 (d, J = 4.6 Hz, 2H), 9.07 (d, J = 5.4 Hz, 2H), 9.03 (d, J = 4.5 Hz, 2H), 8.21 (m, 4H), 7.83 (d, J = 8.2 Hz, 2H), 1.64 (s, 9H), -3.14 (s, 2H). <sup>13</sup>C NMR could not be obtained due to solubility problems. HRMS (MALDITOF): m/z calcd for C<sub>35</sub>H<sub>30</sub>N<sub>5</sub>, 520.2501 [M + H]<sup>+</sup>: found 520.2509. UV-vis (CH<sub>2</sub>Cl<sub>2</sub>):  $\lambda_{\text{max}}/\text{nm}$  ( $\epsilon$ ,  $10^3$ M<sup>-1</sup>cm<sup>-1</sup>) = 407 (341.6), 502 (15.4), 537 (5.8), 574 (5.2), 623 (2.0). IR  $\nu_{\text{max}}/\text{cm}$  · 3278, 2950, 1589, 1535, 1461, 1405, 1240, 1143, 1062, 1049, 971, 956, 848, 782, 736, 688. Anal. Calcd for C<sub>35</sub>H<sub>29</sub>N<sub>5</sub>: C, 80.90; H, 5.63; N, 13.48. Found: C, 80.99; H, 5.57; N, 13.56.

**5-(4-tert-butyl-phenyl)-15-(4-pyridyl)-porphyrin zinc (2a):** Free-baseporphyrin1a (0.168 g, 0.32 mmol) was placed in a 250 mL round-bottom flask and 100 mL of CH<sub>2</sub>Cl<sub>2</sub> was added. The mixture was treated with a MeOH (10 mL) solution of Zn(CH<sub>3</sub>COO)<sub>2</sub>·2H<sub>2</sub>O (0.354 g, 1.6 mmol) and stirred at 40°C for 24h. After solvent evaporation, the residue was extracted with CH<sub>2</sub>Cl<sub>2</sub>/H<sub>2</sub>O (3×50 mL) and then THF (60 mL) was added in the organic phase in order to ensure porphyrin's solubility. The red solution was dried over anhydrous Na<sub>2</sub>SO<sub>4</sub> and the solvent was removed in a rotary evaporator. Metallated porphyrin **2a** was collected as dark purple solid (0.180 g, 95%). mp >300 °C. NMR data could not be obtained due to poor solubility. HRMS (MALDI-TOF): m/z calcd for C<sub>35</sub>H<sub>28</sub>N<sub>5</sub>Zn, 582.1636 [M + H]<sup>+</sup>: found 582.1629. UV-vis (CH<sub>2</sub>Cl<sub>2</sub>/THF: 1/1):  $\lambda_{\text{max}}$ /nm (ε, 10<sup>3</sup>M<sup>-1</sup>cm<sup>-1</sup>) = 412 (399.4), 543 (15.2), 580 (2.8). IR  $\nu_{\text{max}}$ /cm<sup>-1</sup>: 2952, 1600, 1517, 1392, 1355, 1282, 1213, 1145, 1056, 985, 848, 773, 721, 700, 659. Anal. Calcd for C<sub>35</sub>H<sub>27</sub>N<sub>5</sub>Zn: C, 72.11; H, 4.67; N, 12.01. Found: C, 72.22; H, 4.78; N, 11.72.

**5-(4-tert-butyl-phenyl)-10-bromo-15-(4-pyridyl)-20-bromo-porphyrin zinc (3a):** To a solution of zinc-metallatedporphyrin **2a** (0.170 g, 0.29 mmol) in CH<sub>2</sub>Cl<sub>2</sub>/THF (1/1 v/v, 110 mL), a solution of NBS (0.104 g, 0.58mmol)in CH<sub>2</sub>Cl<sub>2</sub> (20 mL) was slowly added at 0°C. The mixture was stirred for 25 min, while checking the reaction progress with TLC, and then acetone (10 mL) was added to quench the reaction. After removing half of the solvent volume under reduced pressure, di-brominated porphyrin **3a** was isolated by filtration as purple, microcrystalline solid (0.131 g, 61%). mp >300 °C.  $^{1}$ H NMR (THF- $^{2}$ - $^{2$ 

5-(4-tert-butyl-phenyl)-15-(4-bipyridyl)-porphyrin (1b): To a degassed CH<sub>2</sub>Cl<sub>2</sub>/MeOH mixture (90/10 v/v, 200 mL), dipyrromethane (0.29 g, 2.00 mmol), bipyridine-4-carbaldehyde (0.18 g, 1.0 mmol) and *tert*-butyl-benzaldehyde (0.17 mL, 1.0 mmol) were successively added under nitrogen in the dark. After 20-min nitrogen bubbling, BF<sub>3</sub>·OEt<sub>2</sub> (1.48 mL, 12.0 mmol) was slowly added in three portions, and the mixture was stirred for 4 days. Then DDQ (0.68 g, 3.0 mmol) was added and the mixture was further stirred for 1 h before addition of Et<sub>3</sub>N (1.68 mL). After 90 min of stirring, the mixture was filtered through silica pad and the filtrate was evaporated to dryness. The crude product was subjected to silica gel column chromatography, using initially CH<sub>2</sub>Cl<sub>2</sub> and then CH<sub>2</sub>Cl<sub>2</sub>/MeOH (9:1) as eluent, from which collecting the second red band isolated the desired asymmetric *trans*-AB

porphyrin. After evaporation of the solvent, the product was further purified by alumina column chromatography with THF/Hex (3:7) as eluent. The solvent was removed and, after washing with *n*-hexane (40 mL), porphyrin **1b** was isolated as red-brown powder (0.055 g, 9%). mp >300 °C.  $^{1}$ H NMR (CDCl<sub>3</sub>, 500 MHz): δ 10.33 (s, 2H), 9.41 (d, J = 4.6 Hz, 2H), 9.40 (d, J = 4.6 Hz, 2H), 9.39 (m, 1H), 9.16 (d, J = 4.6 Hz, 2H), 9.14 (dd,  $J_I$  = 4.8 Hz,  $J_2$  = 0.8 Hz, 1H), 9.10 (d, J = 4.6 Hz, 2H), 8.77 (d, J = 8.1 Hz, 1H), 8.69 (m, 1H), 8.23 (m, 3H), 7.98 (dt,  $J_I$  = 8.0 Hz,  $J_2$  = 1.8 Hz, 1H), 7.83 (d, J = 8.4 Hz, 2H), 7.39 (ddd,  $J_I$  = 7.6 Hz,  $J_2$  = 4.6 Hz,  $J_3$  = 1.2 Hz, 1H), 1.65 (s, 9H), -3.11 (s, 2H).  $^{13}$ C NMR (CDCl<sub>3</sub>, 75 MHz): δ 156.1, 154.8, 151.2, 150.8, 149.6, 147.7, 147.5, 146.3, 145.5, 145.3, 138.3, 137.4, 134.9, 132.4, 131.8, 131.7, 130.4, 130.0, 127.2, 124.2, 124.1, 122.0, 120.4, 115.4, 105.7, 35.1, 31.9.HRMS (MALDI-TOF): m/z calcdfor C<sub>40</sub>H<sub>33</sub>N<sub>6</sub>, 597.2767 [M + H] $^{+}$ : found 597.2778. UV-vis (THF):  $\lambda_{\text{max}}$ /nm ( $\varepsilon$ , 10 $^{3}$ M $^{-1}$ cm $^{-1}$ ) = 406 (320.2), 501 (15.1), 534 (6.3), 574 (5.0), 630 (2.1). IR v<sub>max</sub>/cm $^{-1}$ : 3266, 2952, 1581, 1537, 1457, 1384, 1270, 1241, 1189, 1145, 1093, 1062, 1051, 987, 956, 854, 781, 740, 690, 568. Anal. Calcd for C<sub>40</sub>H<sub>32</sub>N<sub>6</sub>: C, 80.51; H, 5.41; N, 14.08. Found: C, 80.61; H, 5.52; N, 14.19.

5-(4-tert-butyl-phenyl)-15-(4-bipyridyl)-porphyrin zinc (2b): Free-base porphyrin 1b (0.030 g, 0.05 mmol) was placed in a 100 mL round-bottom flask and 20 mL of CH<sub>2</sub>Cl<sub>2</sub>/THF (1:2) was added. The mixture was treated with a MeOH (10 mL) solution of Zn(CH<sub>3</sub>COO)<sub>2</sub>·2H<sub>2</sub>O (0.110 g, 0.5 mmol) and stirred at 50°C for 8h and then at room temperature for 12 h. After solvent evaporation, the residue was extracted with CH<sub>2</sub>Cl<sub>2</sub>/H<sub>2</sub>O (3×50 mL) and then THF (60 mL) was added in the organic phase in order to ensure porphyrin's solubility. The red solution was dried over anhydrous Na<sub>2</sub>SO<sub>4</sub> and the solvent was removed in a rotary evaporator. Metallated porphyrin 2b was collected as a dark purple solid (0.027 g, 93%). mp >300 °C. <sup>1</sup>H NMR (CDCl<sub>3</sub>, 500 MHz): δ 10.23 (s, 2H), 9.38 (t, J = 4.3 Hz, 4H), 9.29 (s, 1H), 9.18 (d, J = 4.3 Hz, 2H), 9.08 (d, J = 4.3 Hz, 2H), 9.06 (d, J = 4.5

Hz, 1H), 8.68 (d, J = 8.0 Hz, 1H), 8.63 (d, J = 3.5 Hz, 1H), 8.18 (m, 3H), 7.95 (t, J = 7.5 Hz, 1H), 7.81 (d, J = 8.0 Hz, 2H), 7.36 (m, 1H), 1.66 (s, 9H). <sup>13</sup>C NMR (CDCl<sub>3</sub>, 125 MHz): δ 156.3, 154.4, 152.4, 150.50, 150.47, 149.7, 149.5, 149.1, 147.6, 139.6, 137.3, 134.7, 134.6, 133.1, 132.3, 131.8, 129.8, 127.1, 124.1, 123.8, 121.9, 121.1, 116.4, 106.5, 35.1, 31.9. HRMS (MALDI-TOF): m/z calcd for  $C_{40}H_{31}N_6Zn$ , 659.1902 [M + H]<sup>+</sup>: found 659.1911. UV-vis (THF):  $\lambda_{max}/nm$  (ε,  $10^3M^{-1}cm^{-1}$ ) = 413 (348.7), 543 (15.1), 580 (8.4). IR  $v_{max}/cm^{-1}$ : 2952, 1585, 1540, 1457, 1390, 1259, 1189, 1147, 1105, 1056, 987, 902, 848, 777, 723, 700, 572. Anal. Calcd for  $C_{40}H_{30}N_6Zn$ : C, 72.78; H, 4.58; N, 12.73. Found: C, 72.86; H, 4.49; N, 12.61. **5-(4-tert-butyl-phenyl)-10-bromo-15-(4-bipyridyl)-20-bromo-porphyrin zinc (3b)**: To a solution of zinc-metallated porphyrin **2b** (0.027 g, 0.04 mmol) in CH<sub>2</sub>Cl<sub>2</sub>/THF (1/2 v/v, 40 mL), a solution of NBS (0.0153 g, 0.08mmol)in CH<sub>2</sub>Cl<sub>2</sub>/THF (1/2 v/v, 10 mL) was slowly added at  $0^{\circ}C$ . The mixture was stirred for 60 min, while checking the reaction progress with TLC, and then acetone (10 mL) was added to quench the reaction. After removing half of the solvent volume under reduced pressure, di-brominated porphyrin **3b** was isolated by filtration

TLC, and then acetone (10 mL) was added to quench the reaction. After removing half of the solvent volume under reduced pressure, di-brominated porphyrin **3b** was isolated by filtration as purple, microcrystalline solid (0.021 g, 64%). mp >300 °C.  $^{1}$ H NMR (THF- $d_8$ , 500 MHz):  $\delta$  9.70 (d, J = 4.7 Hz, 2H), 9.67 (d, J = 4.7 Hz, 2H), 9.37 (m, 1H), 9.06 (d, J = 4.6 Hz, 1H), 8.95 (d, J = 4.7 Hz, 2H), 8.91 (d, J = 4.7 Hz, 2H), 8.87 (d, J = 8.0 Hz, 1H), 8.60 (d, J = 3.8 Hz, 1H), 8.15 (d, J = 3.2 Hz, 1H), 8.11 (d, J = 8.3 Hz, 2H), 7.99 (dt,  $J_1$  = 7.9 Hz,  $J_2$  = 1.8 Hz, 1H), 7.85 (d, J = 8.3 Hz, 2H), 7.38 (m, 1H), 1.65 (s, 9H).  $^{13}$ C NMR (THF- $d_8$ , 75 MHz):  $\delta$  156.9, 155.2, 152.2, 151.7, 151.2, 151.0, 150.9, 150.6, 149.9, 148.1, 140.4, 137.5, 135.3, 135.2, 134.1, 133.9, 133.3, 130.4, 127.0, 124.6, 124.2, 123.6, 121.9, 119.6, 105.3, 35.4, 31.8. HRMS (MALDI-TOF): m/z calcd for  $C_{40}H_{29}Br_2N_6Zn$ , 815.0112 [M + H] $^+$ : found 815.0123. UV-vis (THF):  $\lambda_{max}/nm$  ( $\epsilon$ ,  $10^3$ M $^{-1}$ cm $^{-1}$ ) = 430 (361.6), 565 (15.7), 605 (8.8). IR  $\nu_{max}/cm^{-1}$ : 2946, 1581, 1540, 1454, 1386, 1319, 1282, 1108, 1074, 1022, 997, 908, 865, 808, 788, 730,

670, 574. Anal. Calcd for C<sub>40</sub>H<sub>28</sub>Br<sub>2</sub>N<sub>6</sub>Zn: C, 58.74; H, 3.45; N, 10.28. Found: C, 58.63; H, 3.53; N, 10.39.

**NMR spectra**: <sup>1</sup>H NMR spectra were recorded on Bruker AMX-500 MHz and Bruker DPX-300 MHz spectrometers as solutions in deuterated solvents by using the solvent peak as the internal standard.

**Melting point:** Buchi M-560 melting point instrument was used to for the determination of the melting points of all newly prepared products.

**Masss pectra**: High-resolution mass spectra (HRMS) were recorded on a Bruker Ultrafle Xtreme MALDI-TOF/TOF spectrometer.

FTIR spectra: FTIR were recorded on a Perkin Elmer 16PC FTIR spectrometer.

**X-ray**: Single crystal X-ray crystallographic data were recorded on a STOE IPDS II diffractometer equipped with an image plate detector.

Electrochemistry: Cyclic voltammetry experiments were carried out at room temperature using an Auto Lab PGSTAT20 potentiostat and appropriate routines available in the operating software (GPES, version 4.9). Measurements were carried out in freshly distilled and deoxygenated THF, with a scan rate 100 mV/s, with a solute concentration of 1.0 mM, in the presence of tetrabutylammonium tetrafluoroborate (0.1 M) as supporting electrolyte. A three-electrode cell setup was used with a platinum working electrode, a saturated calomel (SCE) reference electrode, and a platinum wire as counter electrode.

**Photophysical measurements**: UV-vis absorption spectra were recorded on a Shimadzu UV-1700 spectrophotometer using 10 mm path-length cuvettes. Emission spectra were recorded on a JASCO FP-6500 fluorescence spectrophotometer equipped with a red sensitive WRE-343 photomultiplier tube (wavelength range 200-850 nm). For the UV-Vis spectra on TiO<sub>2</sub> film, the TiO<sub>2</sub> (~12 μm) was immersed into a dye solution THF/EtOH (2:1 v/v) mixture containing chenodeoxycholic acid (CDCA, 0.4 mM) for 12 h and then washed. Then the dye

loaded  $TiO_2$  film was put on the sample assembly for thin film absorption in the UV-absorption spectrophotometer and recorded the absorption spectra at the interval of 0.5 nm. For the emission measurements on the  $TiO_2$  films, the films were placed diagonally in an appropriate holder. The excitation beam was directed 45° to the film surface and the emitted light was monitored from the front face of the sample

Computational Methods: Density functional theory (DFT) calculations<sup>57</sup> were performed using the GAUSSIAN 03 program suite.<sup>58</sup> Geometry optimizations in gas phase and in THF were carried out by employing Becke three parameter exchange in conjunction with Lee-Yang-Parr correlation functional (B3LYP).<sup>59, 60</sup> For the geometry optimizations, the LANL2DZ basis set was used for Zn atoms and the 6-31G(d) basis sets for lighter atoms. The input geometries were modeled using the ChemCraft software.<sup>61</sup> The optimized minimum-energy structures were verified as stationary points on the potential energy surface by vibrational frequency analysis calculation. Solvent effects were evaluated by using the polarizable continuum model (PCM) implemented on Gaussian 03, in which the cavity is generated via overlapping spheres, previously developed by Tomasi.<sup>62, 63</sup> Computed structures and molecular orbitals were visualized and analyzed using ChemCraft software.

Cell Fabrication: Electrodes of DSSCs were based on fluorine doped tin oxide (FTO) glass substrates, which were pre-cleaned with deionized water, acetone, and ethanol and then dried in ambient conditions. TiO<sub>2</sub> working electrodes and Pt coated counter electrodes were fabricated as reported earlier.<sup>64</sup> Dye-sensitized photoanodes were obtained by immersing the TiO<sub>2</sub> electrode into 0.3 mM solutions of porphyrins in a THF/EtOH (2:1 v/v) mixture containing chenodeoxycholic acid (CDCA, 0.4 mM) for 12 h. We have used CDCA to reduce the dye aggregation, as most of the porphyrin dye undergoes dye aggregation when adsorbed on to TiO<sub>2</sub> film. The electrodes were assembled into a sealed sandwiched type cell by heating at 80°C with a thermal adhesive film (25 μm thick surlyn) as spacer between the

electrodes. A drop of electrolyte solution containing 0.05 M I<sub>2</sub>, 0.5 M LiI, 0.5 M 1,2-dimethyl-3-n-propylimdazolium iodide and 0.5 M *tert*-butyl-pyridine (TBP) in a CH<sub>3</sub>CN/valeronitrile (85/15 v/v) mixture, was placed space between the electrodes, through a hole predrilled in the counter electrode and then the hole was again sealed with surlyn polymer and cover glass.

Photovoltaic measurements: The current-voltage (*J-V*) characteristics of DSSCs under illumination were measured by a Keithley source meter, and a solar simulator coupled with a 150 W xenon lamp and an AM optical filter to give 100 mW/cm² illumination at the DSSC surface. The active area of the DSSCs was 0.20 cm². Incident photon to current conversion efficiency (IPCE) data were obtained as a function of different wavelengths by using a xenon lamp, a monochromator, and a Keithley source meter under constant illumination intensity at each wavelength. Intensity calibration for IPCE data was performed using a standard silicon photo-diode. Current was measured in short circuit conditions. Electrochemical impedance (EI) spectra, in dark and under illumination, were recorded using an electrochemical workstation (Autolab PGSTAT) with a frequency response analyzer. A frequency range from 10 mHz to 100 kHz and an alternative-current potential of 10 mV were used. A direct-current bias equivalent to the open-circuit voltage of DSSC was applied. Electrochemical impedance spectroscopy (EIS) data were analyzed using Z-View software with an appropriate equivalent circuit

## RESULTS AND DISCUSSION

**Synthesis and characterization**. As shown in Scheme 1, both Znpor-py (**3a**) and Znpor-bpy (**3b**) consist of zinc-metallated porphyrin units which are substituted at opposite 5 and 15 *meso* positions of the macrocyclic rings with a 4-*tert*-butyl-phenyl group and either a pyridyl or a bipyridyl group, while at the other two *meso* positions bromine atoms are present. The pyridyl-containing moieties of both porphyrins have the potential to act as anchoring groups

onto the  $TiO_2$  surface of DSSC electrodes through Lewis acid-base interactions. Considering the 4-*tert*-butyl-phenyl group as electron donating (D) group and the pyridyl-containing moieties as electron accepting (A) groups, both porphyrins can be regarded as dyes with a donor- $\pi$ -acceptor (D- $\pi$ -A) molecular architecture.

The initial step of the synthesis of Znpor-py (3a) involved the preparation of porphyrin 1a (Scheme 2). This 5,15-AB-type porphyrin was synthesized by a mixed condensation reaction of dipyrromethane with two different aldehydes, 65 namely 4-tert-butyl-benzaldehyde and 4pyridyl-aldehyde, which was acid-catalyzed by BF<sub>3</sub>·OEt<sub>2</sub>, in a CH<sub>2</sub>Cl<sub>2</sub>/MeOH mixture for 3 days, followed by addition of DDQ. Due to the fact that the pyridyl group of 4-pyridylaldehyde has the potential to react with BF<sub>3</sub> and reduce its efficiency to catalyze the condensation, it is necessary to use excess BF<sub>3</sub>·OEt<sub>2</sub> and long reaction time. The desired asymmetric product 1a was chromatographically separated and isolated from the statistical mixture of the three different porphyrins that are formed, using silica gel followed by alumina column chromatography and CH<sub>2</sub>Cl<sub>2</sub> as eluent, in 13% yield. Subsequent reaction of 1a with excess of Zn(CH<sub>3</sub>COO)<sub>2</sub>·2H<sub>2</sub>O in MeOH/CH<sub>2</sub>Cl<sub>2</sub>, at 40 °C for 24 h, resulted in the preparation of zinc-metallated porphyrin 2a. Di-brominated porphyrin 3a was obtained in 61% yield, by reaction of 2a with two equivalents of NBS in CH<sub>2</sub>Cl<sub>2</sub> at 0°C. Compound Znporbpy (3b) was prepared following an analogous synthetic route as in the case of porphyrin 3a (Scheme 2). Initially, porphyrin 1b was synthesized by acid catalyzed mixed condensation reaction of dipyrromethane with 4-tert-butyl-benzaldehyde and bipyridyl-4-aldehyde. After metalation reaction with Zn(CH<sub>3</sub>COO)<sub>2</sub>·2H<sub>2</sub>O and bromination reaction with NBS, the final product **3b** was obtained.

**X-ray crystallography.** Single crystals of porphyrin**2b** suitable for X-ray crystallographic analysis were obtained by slow evaporation of a CH<sub>2</sub>Cl<sub>2</sub>/THF solution of **2b**. The compound was crystallized in the form of its THF adduct. Crystal structure and refinement parameters

are given in Table 1. A drawing of the structure is shown in Figure 1, while selected bond distances and angles are listed in Table 2 (full list of bond distances and angles are provided in Table S3 in Supporting Information). The structure consists of a Zn-metallated porphyrin unit in which the metal atom is coordinated by four pyrrole N-atoms. The Zn-N (pyrrole) bond lengths were found to be within the range of 2.053-2.065Å. In general, a 4-coordinate Zn metal atom located in the center of a porphyrin unit has the ability to bind Lewis bases on both sides of the molecular framework. In the present case, there is only one THF solvent molecule axially coordinated on one side, with a Zn-O1 distance of 2.190(2) Å, resulting in a 5-coordinate, square-pyramidal geometry. The THF molecule was found to exhibit a two-fold orientation disorder (Figure S1). In this coordination environment, the Zn metal atom appears to deviate from the mean plane of the pyrrole N-atoms by 0.22 Å, as it has typically been observed in related structures. <sup>66, 67</sup> The 4-tert-butyl-phenyl and bipyridyl groups located at opposite positions at the periphery of the porphyrin macrocycle were found to be in an almost perpendicular orientation with respect to the porphyrin framework, with dihedral angles of ~95° and ~110°, respectively.

**Photophysical properties**. UV-Vis absorption spectra of Znpor-py (**3a**) and Znpor-bpy (**3b**) in THF solutions are shown in Figure 2 (black color). Both compounds exhibit similar absorption profiles with typical porphyrin absorption characteristics, which include a strong Soret band appearing at 400-450 nm and moderate Q-bands at 550-650 nm. These are attributed to  $\pi$ - $\pi$ \* transitions within the D- $\pi$ -A conjugated macrocyclic porphyrin rings.<sup>20</sup>

The absorption spectra of porphyrins **3a** and **3b** adsorbed onto TiO<sub>2</sub> films were also recorded (Figures **2a** and **2b**, red color). Both porphyrins show similar absorption profiles, indicating that their light harvesting efficiencies are very similar. Furthermore, the Soret and Q-absorption bands of the adsorbed dyes on TiO<sub>2</sub> films appear broader and red-shifted, with respect to the corresponding solution spectra. The broadening of the absorption bands is

attributed to the electronic coupling between the dyes and the  $TiO_2$  semiconductor. <sup>68-71</sup> Furthermore, the absorption characteristics of the adsorbed dyes provide information for their aggregation morphology on the  $TiO_2$  electrode. *H*-aggregates, in which molecules are aligned parallel to each other with strong intermolecular interactions, tend to induce a non-radiative deactivation process<sup>72</sup> and leads to blue shift of the absorption bands. In contrast, *J*-aggregates, in which the molecules are arranged in a head-to-tail direction, induce relatively high fluorescence efficiency with a bathochromic shift in optical absorption band. The redshift observed in the absorption bands of the two porphyrins **3a** and **3b** is thought to result from the formation of *J*-aggregates on the  $TiO_2$  surface (shown for **3a**/ $TiO_2$  in Scheme 3).

The fluorescent emission spectra of porphyrins **3a** and **3b** in THF were also recorded and shown in Figure 3. Both the porphyrins exhibit two peaks of unequal intensities at 612 nm and 672 nm, respectively, upon excitation at 565 nm. We have also recorded the fluorescent emission spectra of porphyrins adsorbed onto TiO<sub>2</sub> film as shown in Figure 3. After the adsorption of porphyrin dye onto TiO<sub>2</sub> film, the fluorescence bands were slightly red-shifted and broadened as compared to those of the dyes in solutions. The red-shift of the fluorescence is probably due to the interaction with the nanoparticles (anchoring effect) or with other dye molecules.

**Electrochemistry**. In order to study the feasibility of electron injection and dye regeneration processes in the Znpor-py (**3a**) and Znpor-bpy (**3b**) sensitized solar cells, cyclic voltammetry measurements of the two porphyrins in THF solutions, using tetrabutyl ammonium tetrafluoroborate as supporting electrolyte, were performed. As shown in the cyclic voltammograms in Figure 4, both porphyrins **3a** and **3b** exhibit one oxidation process, at  $E_{1/2}^{\text{ox}} = +1.23$  and +1.21 V vs SCE, respectively, which corresponds to removal of an electron from the  $\pi$ -ring system of the zinc-porphyrin, resulting in the formation of the corresponding porphyrin radical cation, and one reduction process, at  $E_{1/2}^{\text{red}} = -1.11$  and -1.09

V vs SCE, respectively, which is attributed to the reduction of the porphyrin unit, forming a porphyrin radical anion.

For efficient electron injection from the excited state of a sensitizer into the TiO<sub>2</sub> conduction band of a DSSC, the LUMO energy level of the sensitizer (which corresponds to its first reduction potential) should be higher (more negative) than the TiO<sub>2</sub> conduction band edge (-0.74 V vs SCE). Both porphyrins3a and3b exhibit E<sub>1/2</sub><sup>red</sup> values, which are more negative than TiO<sub>2</sub> conduction band edge, suggesting there is sufficient driving force for electron injection from their excited state into the TiO<sub>2</sub> conduction band. On the other hand, in order to ensure efficient regeneration of sensitizer (after electron injection) in a DSSC, the HOMO energy level (which corresponds to its first oxidation potential) should be lower (more positive) than the redox potential of the electrolyte employed in the DSSC (0.4 V vs SCE for I<sub>3</sub>/I). The oxidation potentials of both porphyrins 3a and 3b are more positive than the corresponding electrolyte redox potential, and therefore, regeneration of porphyrin dyes, after the electron injection, is thermodynamically feasible.<sup>73</sup>

**DFT calculations**. In order to gain insight into the molecular and electronic structures of Znpor-py (**3a**) and Znpor-bpy (**3b**), DFT calculations at the B3LYP/6-31G(\*) level of theory were performed in THF. The geometry-optimized structures of the two porphyrins are depicted in Figure 5, while their optimized coordinates are provided in Table S7 and S8 (Supporting Information). Both compounds display a planar central scaffold, which is in accordance with p- $\pi$  conjugated systems, with the Zn atoms being coplanar with the four pyrrole rings. The meso-substitutents, 4-*tert*-butyl-phenyl and either pyridyl or bipyridyl groups, are in an almost perpendicular orientation with respect to the corresponding porphyrin frameworks. In the case of both dyes **3a** and **3b**, the dihedral angles of 4-*tert*-butyl-phenyl and pyridyl group regarding the porphyrin ring were found ~67°. The electron density distributions of the frontier and near frontier molecular orbitals of compounds **3a** and **3b** are

shown in Figure 6. In general, they are primarily extended over the zinc-porphyrin units and partly delocalized over the corresponding meso-substituents. For example, in case of Znporbpy (**3b**) (the porphyrin with the better photovoltaic performance), HOMO-1, HOMO, LUMO, and LUMO+1 are essentially porphyrin-based  $\pi$  molecular orbitals, which is in agreement with the Gouterman's four orbital model of porphyrins. Furthermore, in HOMO and HOMO-2 there are additional contributions over the 4-*tert*-butyl-phenyl group, while in LUMO+1 and LUMO+2 there is significant delocalization over the bipyridyl group. Similar electron density distributions of the frontier molecular orbitals were also found for Znpor-py (**3a**) (Figure 6). Therefore, the calculated electron density distributions of both compounds favor intramolecular electron transfer, upon photoexcitation, from the 4-*tert*-butyl-phenyl donor (D) group to the pyridyl acceptor/anchoring (A) groups through the porphyrin  $\pi$  system (which is consistent with the D- $\pi$ -A description of the two compounds), and promote electron injection, upon their binding onto TiO<sub>2</sub>.

The calculated dipole moments  $\mu$  of Znpor-py (**3a**) and Znpor-bpy (**3b**) were found to be 4.58 and 5.57 D, respectively (Table 3). The larger  $\mu$  value for the latter implies an enhanced ability for directed intramolecular electron transfer and electron injection into TiO<sub>2</sub>, which is in accordance with the observed longer electron lifetime and enhanced photovoltaic performance of the corresponding solar cell (see electrochemical impedance spectroscopy and photovoltaic measurements results).

The theoretically calculated HOMO-LUMO gaps for 3a and 3b in THF were found to be 2.719 eV, which are not significantly deferent from the HOMO-LUMO gaps estimated from cyclic voltammetry measurements.

**FTIR spectra**. To get structural information on the attachment of Znpor-py (**3a**) and Znpor-bpy (**3b**) on the TiO<sub>2</sub> surface of DSSCs, FTIR spectra of the two dyes in neat form and when adsorbed on TiO<sub>2</sub> films were recorded (as shown in Figure 7 for **3a** and **3a**/TiO<sub>2</sub>). The

spectra of both porphyrins in pure form exhibit similar absorption characteristics, with bands for the stretching vibrations of C=C and C-N at 1602 and 1452 cm<sup>-1</sup> for **3a** and 1581 and 1454 cm<sup>-1</sup> for **3b**. Upon adsorption of the porphyrins onto TiO<sub>2</sub>, a new absorption band appears at 1634 cm<sup>-1</sup>, which can be assigned to the pyridyl group coordinated to a Lewis acid site of the TiO<sub>2</sub> surface.<sup>48, 75</sup>

**Photovoltaic performance**. Current-voltage (J-V) characteristics of the DSSCs sensitized by Znpor-py (**3a**) and Znpor-bpy (**3b**) are shown in Figure 8a, while the corresponding photovoltaic parameters are compiled in Table 4. The optimum values of the short circuit current  $J_{\rm sc}$ , open circuit voltage  $V_{\rm oc}$ , and fill factor FF parameters were found to be 8.58 mA/cm<sup>2</sup>, 0.63 V and 0.66 for the **3a**-based solar cell, and 10.52 mA/cm<sup>2</sup>, 0.69 V, and 0.70 for the **3b**-based solar cell, which correspond to overall PCE values of 3.57 and 5.08%, respectively.

A principal reason for the higher PCE value of the **3b**-based solar cell is its higher  $J_{sc}$  value, which is reflected in its higher incident photon-to-electron conversion efficiency (IPCE) response. The IPCE spectra of the two solar cells are shown in Figure 7b. In general, they exhibit very similar IPCE profiles (as shown in the normalized IPCE spectra of the DSSCs in the inset of Figure 8b), but the IPCE response of the solar cell sensitized by **3b** is higher than the IPCE response of the solar cell sensitized by **3a**. In general, the monochromatic IPCE for a DSSC is given by the expression<sup>7,76</sup>

$$IPCE(\lambda) = \eta_{LHE} \eta_{inj} \eta_{cc}$$

where  $\eta_{LHE}$  is the light harvesting efficiency (which is related to the absorption profile of the sensitizing dye and the amount of dye adsorbed onto the TiO<sub>2</sub> surface),  $\eta_{inj}$  is the electron injection efficiency (which is related to the electron injection rate from the excited state of the sensitizer into the TiO<sub>2</sub> conduction band), and  $\eta_{cc}$  is the charge collection efficiency (which is related to the recombination rate of injected electrons with the oxidized dye or redox couple

in the electrolyte). We have measured the dye loading onto the TiO<sub>2</sub> film using dye desorption method and found the this is about 3.4x10<sup>-7</sup> mol/cm<sup>2</sup> and 3.12 x10<sup>-7</sup> mol/cm<sup>2</sup> for 3a and 3b, respectively. Considering that the dye loading is similar for both the dyes leading to similar LHE, we assume that the major factors that lead to a higher IPCE response for the **3b**-based solar cell should be  $\eta_{inj}$  and  $\eta_{cc}$ . This can justified by the chemical structures of the two sensitizers, since 3b can be considered to be a molecule with a double-pyridine anchoring group, compared to the single pyridine group of 3a, which has the potential coordinate stronger and increase the interfacial electron transfer process, and therefore leading to a higher  $\eta_{inj}$  value. Moreover, both DSSCs showed two times higher IPCE value at the Soret band than at the Q bands. This could be attributed to better overlapping between the LUMO+2 and LUMO+3 orbitals of the porphyrins and the TiO<sub>2</sub> conduction band when both dyes were excited at the of the Soret band wavelengths. As can be seen in the fluorescence spectra of porphyrin dyes adsorbed on TiO<sub>2</sub> (Figure 3), the fluorescence intensity was more quenched for 3b porphyrin as compared to 3a, also suggested the photo-induced charge transfer is more pronounced in for later, leading to higher  $J_{sc}$  and PCE for 3b sensitized DSSC.

The enhanced photovoltaic performance of the **3b**-based solar cell is also related to its enhanced  $V_{\rm oc}$  parameter. In general, the  $V_{\rm oc}$  value of DSSC is determined by the potential difference between the quasi Fermi level of TiO<sub>2</sub> (E<sub>CB</sub>) and the HOMO energy level of the redox couple ( $E_{\rm redox}$ ) in the electrolyte, as described by the following relationship.<sup>77</sup>

$$V_{oc} = \frac{E_{CB}}{q} + \frac{kT}{q} \ln \left( \frac{N_{CB}}{n} \right) - \frac{E_{redox}}{q}$$

Where k is the Boltzmann's constant, T is the temperature, q is the electronic charge,  $N_{CB}$  is the effective electron density of states at  $TiO_2$  conduction band edge, n is the concentration of injected electrons in  $TiO_2$  conduction band edge. Since the same electrolyte redox couple

was used for both 3a- and 3b-based DSSCs, their different  $V_{oc}$  values result from differences in the quasi Fermi level of  $TiO_2$  conduction band. The quasi Fermi level of  $TiO_2$  is influenced by the balance between electron injection and charge recombination, i.e. the number of electrons in the  $TiO_2$  conduction band. The higher  $V_{oc}$  value of the 3b-sensitized DSSC could be attributed to a larger number of electrons in the  $TiO_2$  conduction band, which results from a more effective interfacial electron injection caused by the bipyridine anchoring group. In addition, the higher  $V_{oc}$  value of the solar cell sensitized by 3b is also determined by the recombination rate of the injection electrons with the redox active species of the electrolyte ( $I_3$ ), as discussed in the following paragraphs.

To shed light in the relationship between the electron transfer kinetics and the corresponding photovoltaic properties of the two DSSCs, electrochemical impedance spectroscopy (EIS) measurements were carried out. The Nyquist and Bode plots for the two DSSCs in dark, under a forward bias of -0.64 V, are shown in Figures 9a and 9b, respectively. The Nyquist plots of both solar cells show three semicircles in the frequency ranges 10<sup>5</sup>-10<sup>3</sup>, 10<sup>3</sup>-1, and 1-10<sup>-2</sup> Hz which corresponds to impedances at counter electrode/electrolyte interface, TiO<sub>2</sub>/dye/electrolyte interface, and diffusion process in electrolyte, respectively. 78, 79 The larger radius of the middle frequency semicircle signal of the 3b-sensitized solar cell, compared to that of the 3a-based solar cell, indicates a higher charge recombination resistance ( $R_{\text{rec}}$ ) at the TiO<sub>2</sub>/dye/electrolyte interface (63 vs 42 $\Omega$ cm<sup>2</sup>, respectively). In other words, the 3b-based solar cell exhibits a slower charge recombination rate, which leads to a more effective charge recombination retardation between injected electron into the TiO2 conduction band and oxidized species (I3-) in the electrolyte. The characteristic middle frequency signal in the Bode phase plot of a DSSC is also related to the charge recombination rate. In particular, the reciprocal of the peak frequency maximum  $(f_{\text{max}})$ of this signal is related to electron lifetime ( $\tau_e$ ) according to the relationship

$$\tau_e = \frac{1}{2\pi f_{\text{max}}}$$

As shown in Figure 9b, the peak frequency for the **3b**-based solar cell is lower than that for the **3a**-based solar cell, which leads to a longer electron lifetime for the former cell (31vs 18ms for **3b** and **3a**, respectively). In other words, the DSSC sensitized by **3b** exhibits a slower charge recombination rate, which is consistent with the presence of the bipyridine anchoring group in the molecular structure of **3b** that offers more pathways for electron injection into the TiO<sub>2</sub> conduction band, compared to the simple pyridine group in **3a**.

These results are further supported by measurement of the J-V characteristics of the two DSSCs under dark conditions (Figure 10), since the dark current is a measure of the recombination process in a DSSC. Due to the fact that the dark current of the **3b**-based DSSC is found to be lower than that of the **3a**-based DSSC, the former device exhibits a higher charge recombination resistance at the  $TiO_2/dye/electrolyte$  interface.

As mentioned above, the reason for the enhanced photovoltaic performance of the **3b**-sensitized solar cell, compared to the **3a**-based solar cell, can be associated with the molecular structures of the corresponding sensitizers. Since the two porphyrins exhibit very similar light absorption characteristics, their difference results only from the anchoring groups they use for attachment to the TiO<sub>2</sub> photoanodes. Both compounds are bound to the acid sites of TiO<sub>2</sub> through their N(pyridyl) atoms. It has been recently shown that N(pyridyl) containing anchoring groups provide efficient adsorption of the sensitizers onto the TiO<sub>2</sub> surface and support an excellent electronic coupling between the levels of the excited sensitizer and those of TiO<sub>2</sub>. <sup>34, 50</sup> The presence of bipyridyl group in **3b**, which offers two effectively bound pyridyl groups, in contrast to only one pyridyl group in **3a**, results in more effective binding and formation of a more compact layer of **3b** onto the TiO<sub>2</sub> surface, and provides more electron transfer pathways to the TiO<sub>2</sub> surface, leading to a faster and more efficient electron injection process (Scheme 4), which is demonstrated by its longer electron

lifetime. The coordination geometries of the two dyes onto to TiO<sub>2</sub> surface might also play a significant role. The presence of a pyridyl group in Znpor-py (**3a**) results in a perpendicular edge-to-face attachment of the porphyrin unit with respect to the TiO<sub>2</sub> surface, while in case of Znpor-bpy (**3b**), the two pyridyl groups of the bipyridyl anchoring moiety result in a coordination geometry with a slightly tilted porphyrin unit with respect to the TiO<sub>2</sub> surface. Considering that in both cases porphyrin units from *J*-aggregates upon their adsorption onto TiO<sub>2</sub> (see Photophysical measurements), in case of the **3b**-sensitzed solar cell the tilted porphyrin units form a more compact hydrophobic layer at the TiO<sub>2</sub> surface than in the **3a**-based solar cell, which causes retardation of the I<sub>3</sub><sup>-</sup> diffusion onto the TiO<sub>2</sub> electrode and results in a more effective suppression of charge recombination (RC) between the injected electron and electrolyte redox couple (Scheme 4). Nevertheless, advanced spectroscopic techniques, in combination with computational studies, are needed in order to investigate in detail the relationship between adsorption geometry and electron transfer between the adsorbed porphyrin unit and the TiO<sub>2</sub> surface.

### **CONCLUSIONS**

Herein, we present the synthesis of two porphyrins with the D- $\pi$ -A molecular architecture, which are functionalized with terminal pyridyl and bipyridyl acceptor groups, namely Znporpy (**3a**) and Znpor-bpy (**3b**). The *N*-containing units of the two porphyrins have the potential to act as anchoring groups on the TiO<sub>2</sub> surface, while photophysical and electrochemical measurements of the two compounds, supported by theoretical DFT calculations, revealed the presence of suitable HOMO and LUMO energy levels for utilization as sensitizers in DSSCs. Photovoltaic measurements of the corresponding DSSCs showed an enhanced photovoltaic performance for the Znpor-bpy (**3b**)-sensitized solar cell, as a result of its higher short circuit current  $J_{sc}$  and open circuit voltage  $V_{oc}$  parameters. This was attributed to the more effective

binding of the bipyridine anchoring group onto the  $TiO_2$  surface and the formation of a more compact dye layer on the Znpor-bpy (**3b**) based solar cell photoanode, which result in higher charge injection efficiency, and more effective suppression of recombination of the injected electrons with  $I_3^-$  in the electrolyte. These arguments are supported by EIS measurements, which show higher charge recombination resistance  $R_{rec}$ , and longer electron lifetime  $\tau_e$  for the Znpor-bpy (**3b**)-based solar cell.

### ASSOCIATED CONTENT

**Supporting Information**. CIF for **2b** (THF), ORTEP diagram and Tables with X-ray crystallographic information for **2b** (THF), <sup>1</sup>H NMR and <sup>13</sup>C NMR spectra of compounds **1a**, **2a**, **3a**, **1b**, **2b**, and **3b**, and optimized coordinates from DFT calculations for **3a** and **3b**.

### **AUTHOR INFORMATION**

### **Corresponding Authors.**

\*E-mail: coutsole@chemistry.uoc.gr (A.G.C.); gdsharma273@gmail.com (G.D.S.).

### **ACKNOWLEDGEMENT**

Financial support from the European Commission (FP7-REGPOT-2008-1, Project BIOSOLENUTI No 229927) and the Special Account for Research of the University of Crete are greatly acknowledged.

**Table 1.** Crystal structure and refinement parameters for **2b** (THF).

empirical formula	C <sub>44</sub> H <sub>38</sub> N <sub>6</sub> OZn	$C_{44}H_{38}N_6OZn$			
formula weight	732.17	732.17			
crystal system	monoclinic	monoclinic			
space group	C2/c				
unit cell dimensions	a = 21.201(7)  Å	α= 90°			
	b = 10.863(2)  Å	β= 98.94(4)°			
	c = 32.160(6)  Å	$\gamma = 90^{\circ}$			
volume	7317(3) Å <sup>3</sup>				
Z	8	8			
density (calculated)	1.329 g/cm <sup>3</sup>	1.329 g/cm <sup>3</sup>			
absorption coefficient	0.715 mm <sup>-1</sup>	0.715 mm <sup>-1</sup>			
reflections collected	47595	47595			
data / restraints / parameters	9536 / 0 / 509				
final R indices [I>2sigma(I)]	R1 = 0.0680, wR2 = 0	R1 = 0.0680, wR2 = 0.0981			
goodness-of-fit on F <sup>2</sup>	1.035	1.035			

**Table 2.** Selected bond distances and angles for **2b** (THF).

	Во	nd distances (Å)		
Zn1-N1	2.053(3)	Zn1-N4	2.065(3)	
Zn1-N3	2.055(3)	Zn1-O1	2.190(2)	
Zn1-N2	2.062(3)			
	Вс	ond angles (deg)		
N1-Zn1-N3	165.88(9)	N3-Zn1-N4	89.93(11)	
N1-Zn1-N2	90.13(12)	N2-Zn1-N4	168.88(9)	
N3-Zn1-N2	88.43(12)	N1-Zn1-O1	95.50(11)	
N1-Zn1-N4	88.77(12)	N3-Zn1-O1	98.61(11)	
C6-C5-C21-C22 95.1(4)		C14-C15-C31-C32	113.9(4)	

**Table 3.** DFT calculated properties of Znpor-py (**3a**) and Znpor-bpy (**3b**).

HOMO/eV	LUMO/eV	HOMO-LUMO gap/eV	Dipole moment μ/D	
-5.353	-2.634	2.719	4.58	
-5.360	-2.641	2.719	5.57	
	-5.353	-5.353 -2.634	-5.353 -2.634 2.719	

Table 4. Photovoltaic and electrochemical impedance spectroscopy parameters of DSSCs sensitized by Znpor-py (3a) and Znpor-bpy (3b).

DSSC sensitized by:	$J_{ m sc}/{ m mA/cm}^{2[a]}$	$V_{ m oc}^{ m [b]}/ m V$	$FF^{[c]}$	PCE/% <sup>[d]</sup>	$R_{\rm rec}/\Omega{ m cm}^{2[{ m e}]}$	$R_{\rm tr}/\Omega { m cm}^{2[{ m f}]}$	τ <sub>e</sub> /ms <sup>[g]</sup>
Znpor-py (3a)	8.58	0.63	0.66	3.57 (3.48) <sup>[i]</sup>	42	34	18
Znpor-bpy ( <b>3b</b> )	10.52	0.69	0.70	5.08 (4.96) <sup>[i]</sup>	63	23	31

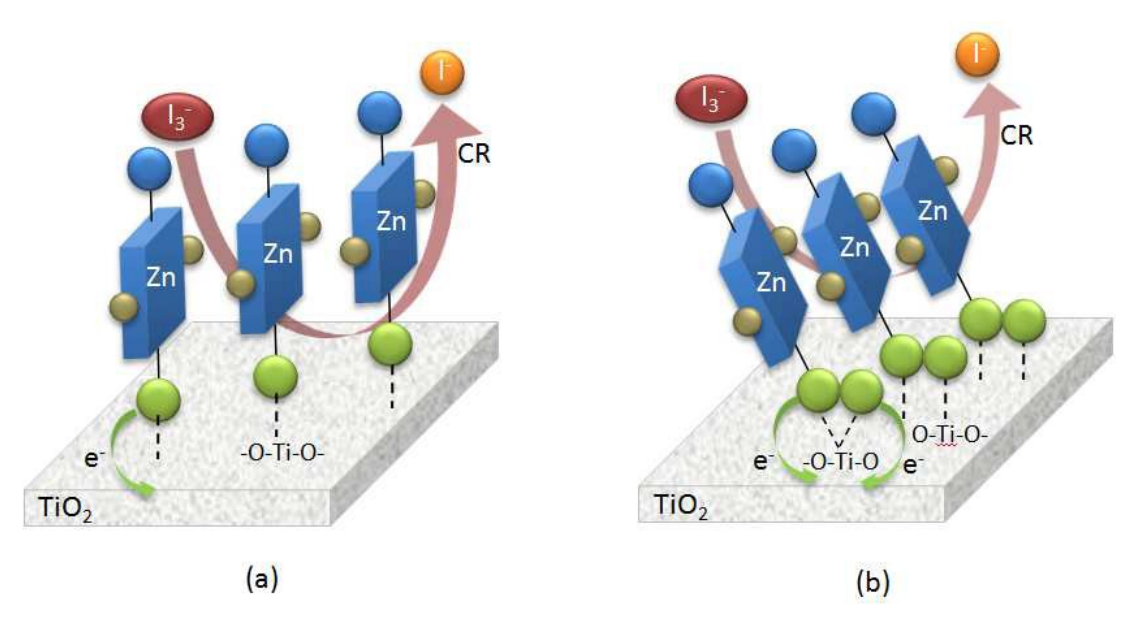
[a] short circuit current, [b] open circuit voltage, [c], fill factor, [d] photoconversion efficiency, [e] charge recombination resistance at the  $TiO_2/dye/electrolyte$  interface, [f] charge transport resistance, [g] electron lifetime and [i] average of eight devices.

Scheme 1. Chemical structures of Znpor-py (3a) and Znpor-bpy (3b).

Scheme 2. Synthetic routes for the preparation of Znpor-py (3a) and Znpor-bpy (3b).

$$\frac{1}{2n} = \frac{1}{2n}$$

Scheme 3. Schematic representation of J-aggregate formation for Znpor-py (3a) when attached onto  $TiO_2$  film.



Scheme 4. Schematic representation of the attachment of (a) Znpor-py (3a) and (b) Znpor-bpy (3b) onto TiO<sub>2</sub>.

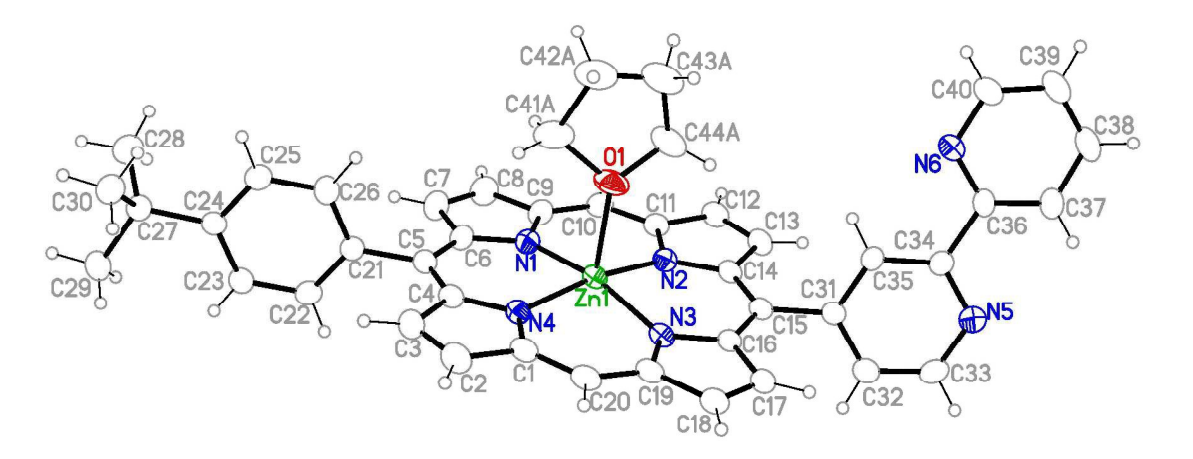


Figure 1. ORTEP representation of X-ray crystal structure of **2b** THF) with all atoms represented by thermal ellipsoids at the 35% probability level.

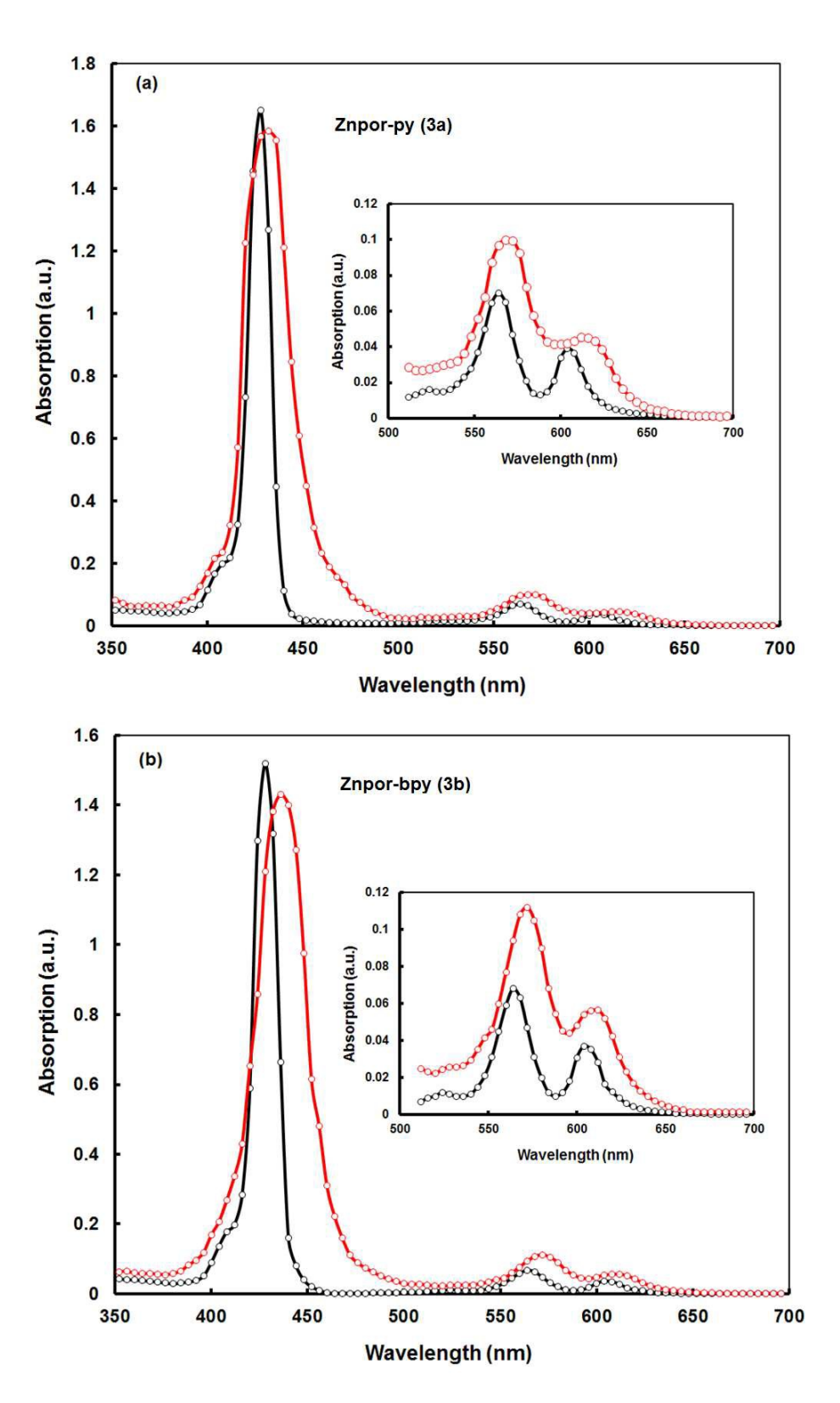


Figure 2. UV-Vis absorption spectra of (a) Znpor-py (3a) and (b) Znpor-bpy (3b) in THF solutions (black color) and adsorbed onto TiO<sub>2</sub> films (red color).

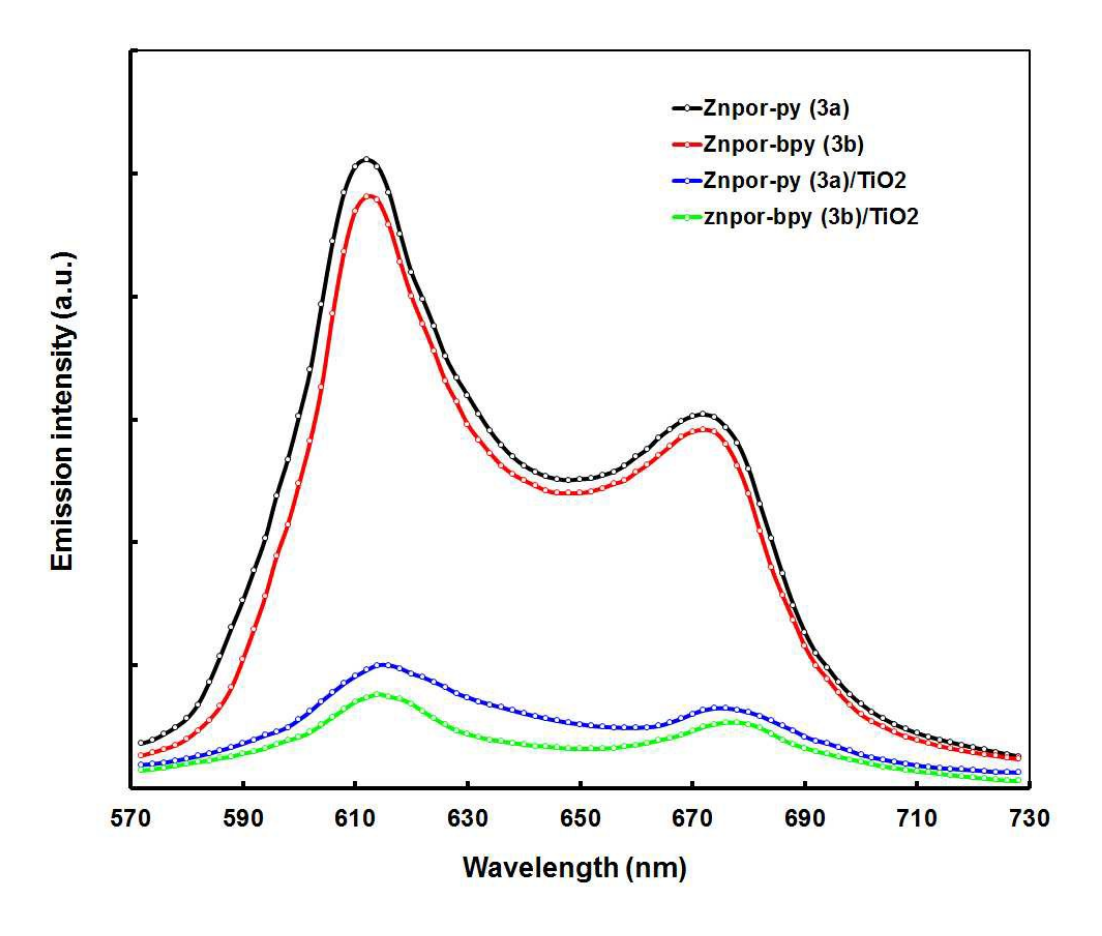


Figure 3. Fluorescence spectra of Znpor-py (3a) (black color) and Znpor-bpy (3b) (red color) in isoabsorbing THF solutions and absorbed onto TiO2 film (Znpor-py (3a) (blue color) and Znpor-bpy (3b) (green color) upon excitation at 565 nm

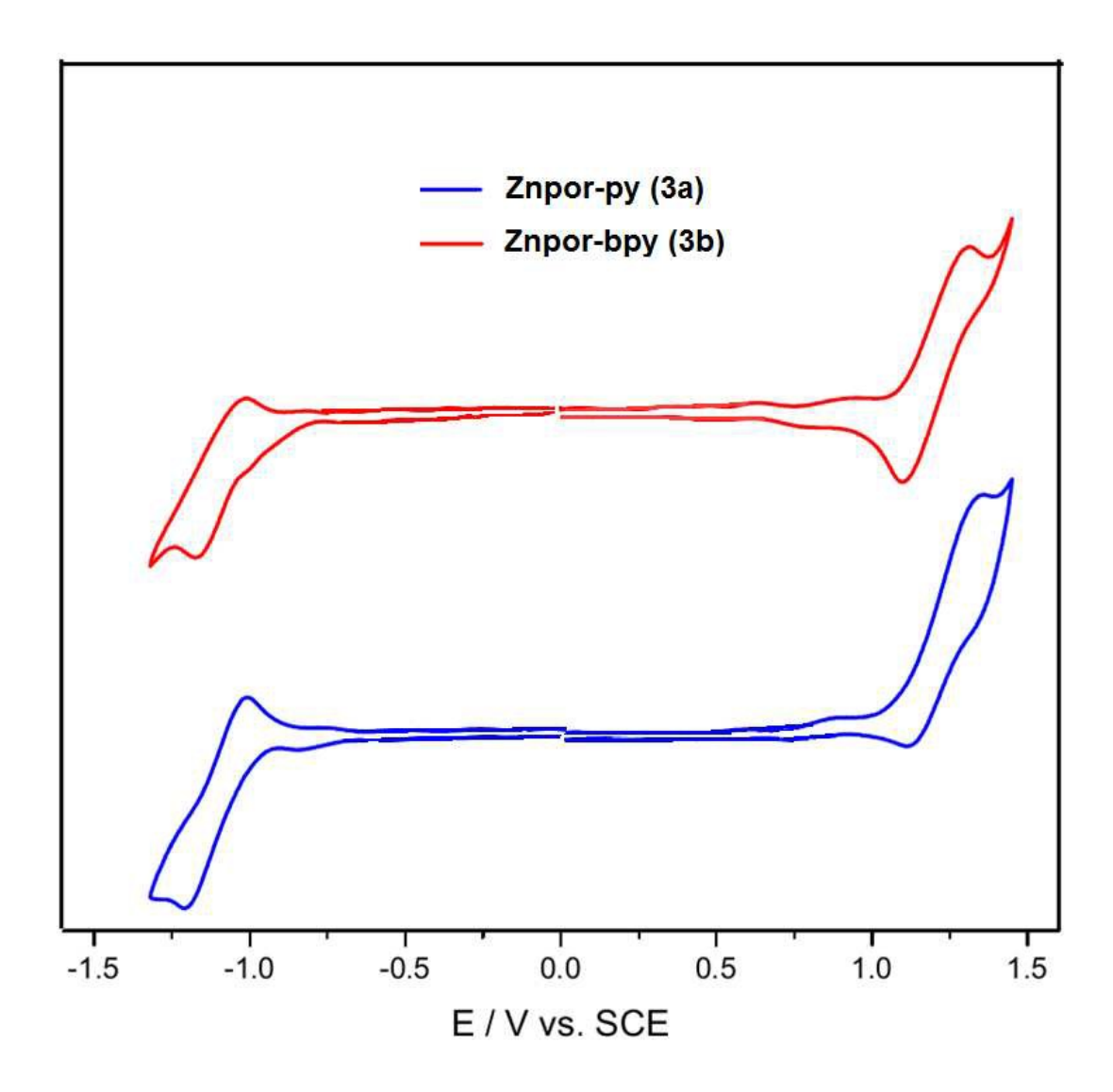


Figure 4. Cyclic voltammograms of Znpor-py (3a) (blue color) and Znpor-bpy (3b) (red color) in THF solutions.

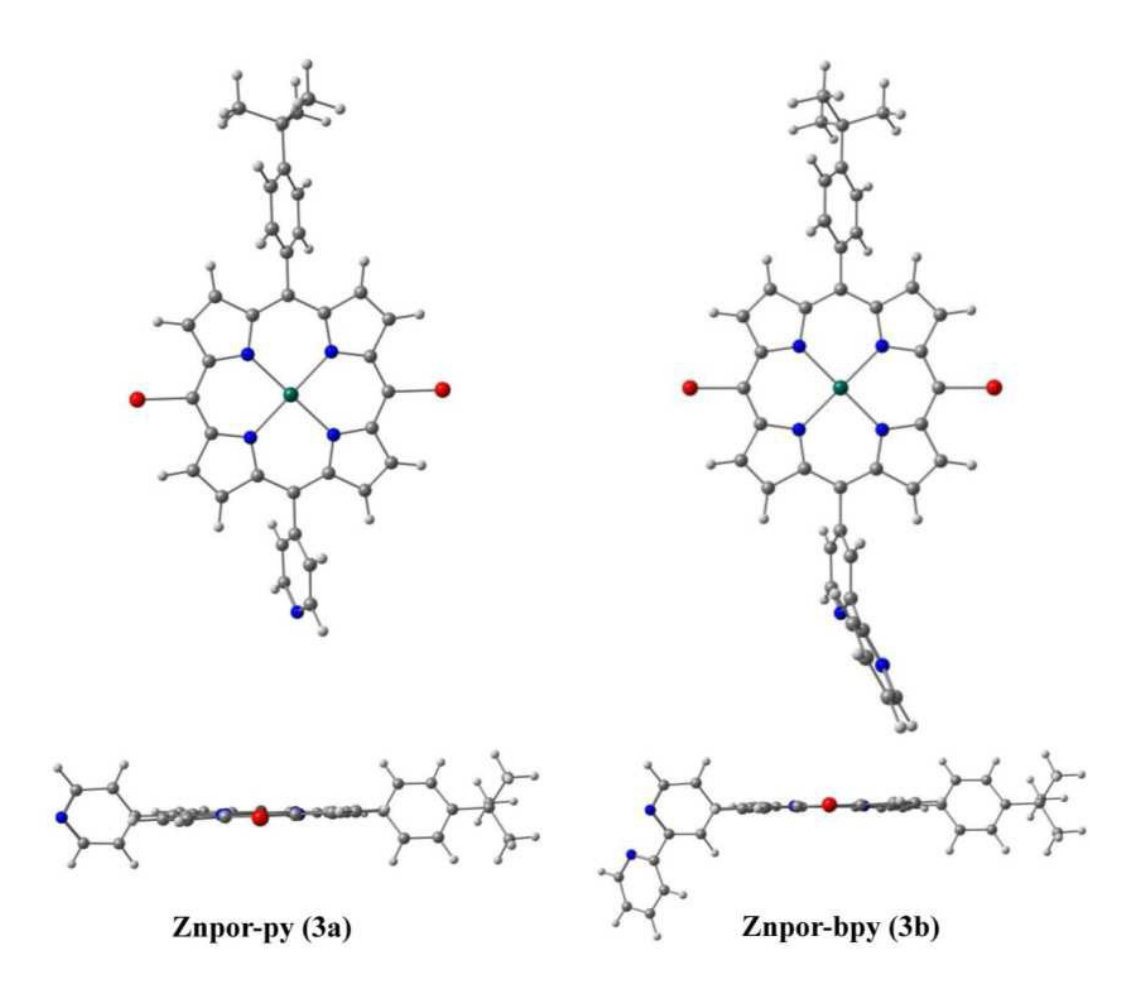


Figure 5. Different views of geometry optimized structures of Znpor-py (3a) and Znpor-bpy (3b) in THF. Carbon, nitrogen, hydrogen, bromine and zinc atoms correspond to grey, blue, white, red, green spheres, respectively.

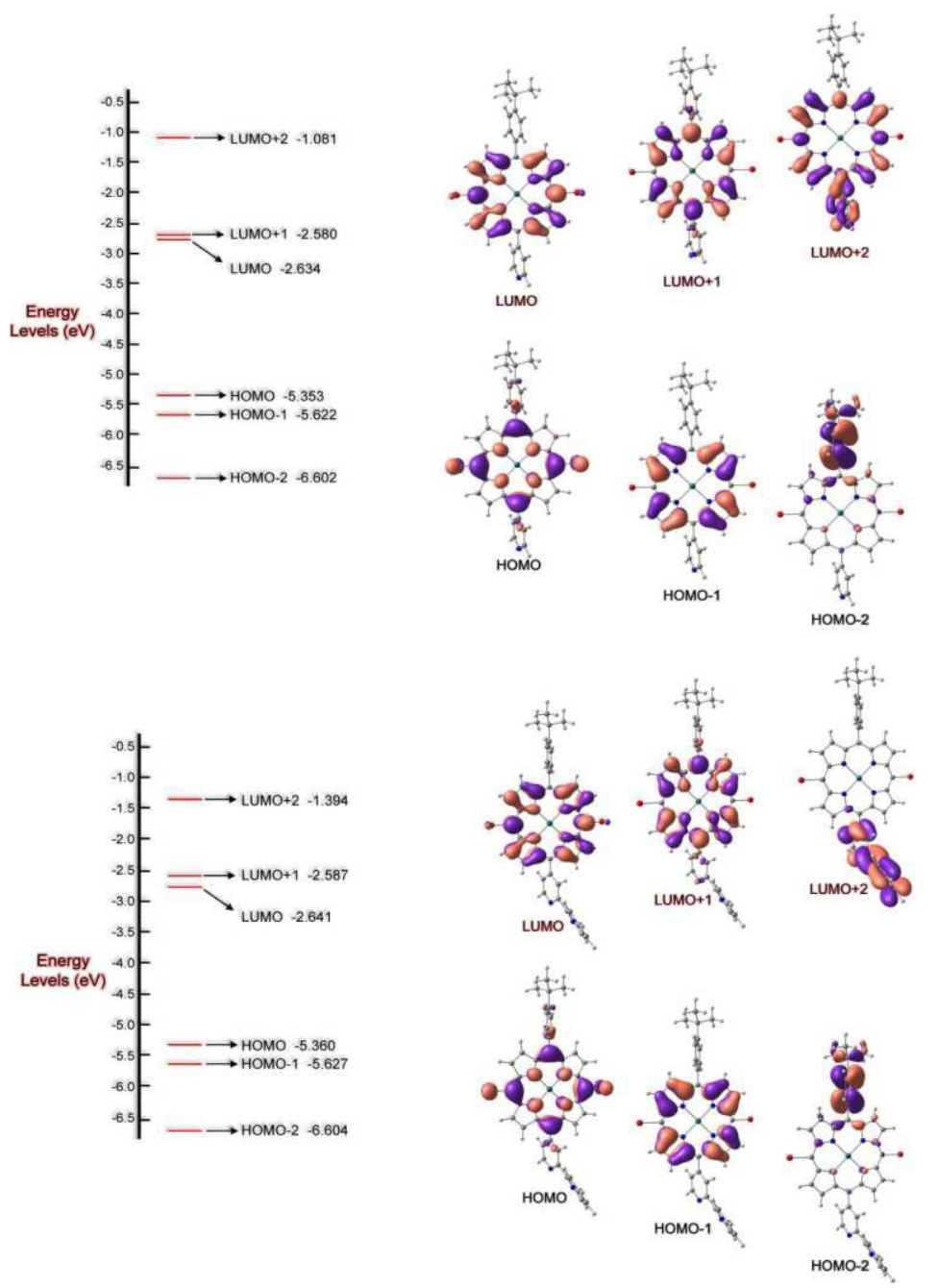


Figure 6. Frontier molecular orbitals of Znpor-py(3a) (upper part) and Znpor-bpy (3b) (lower part) and their corresponding energy levels calculated in THF.

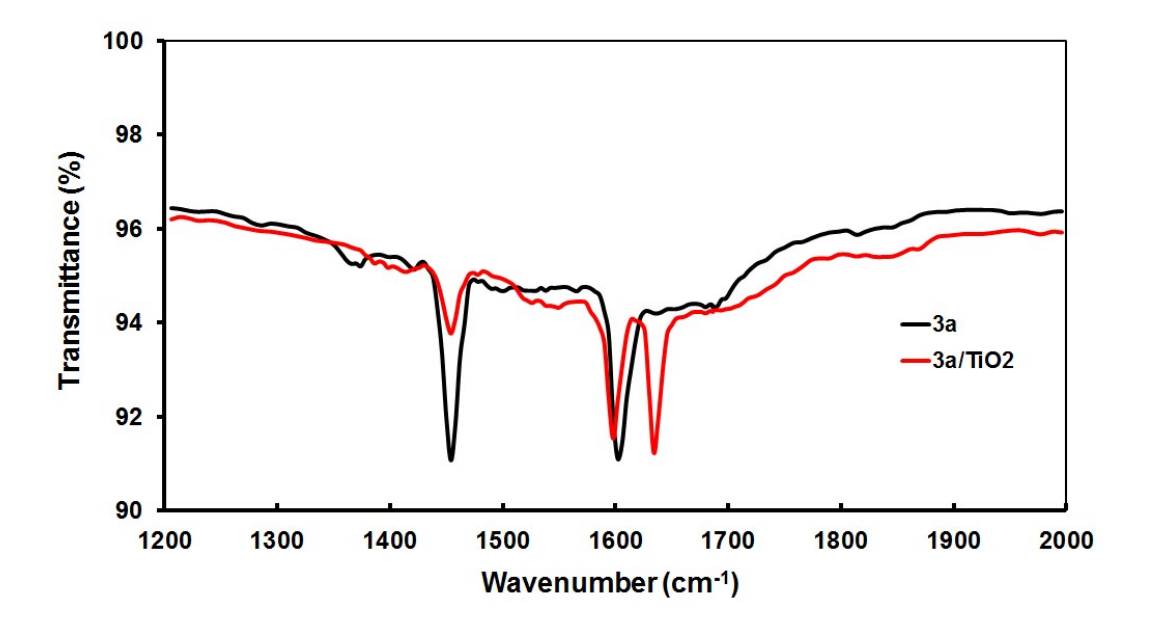


Figure 7. FTIR spectra of pristine 3a and 3a adsorbed onto TiO<sub>2</sub> film

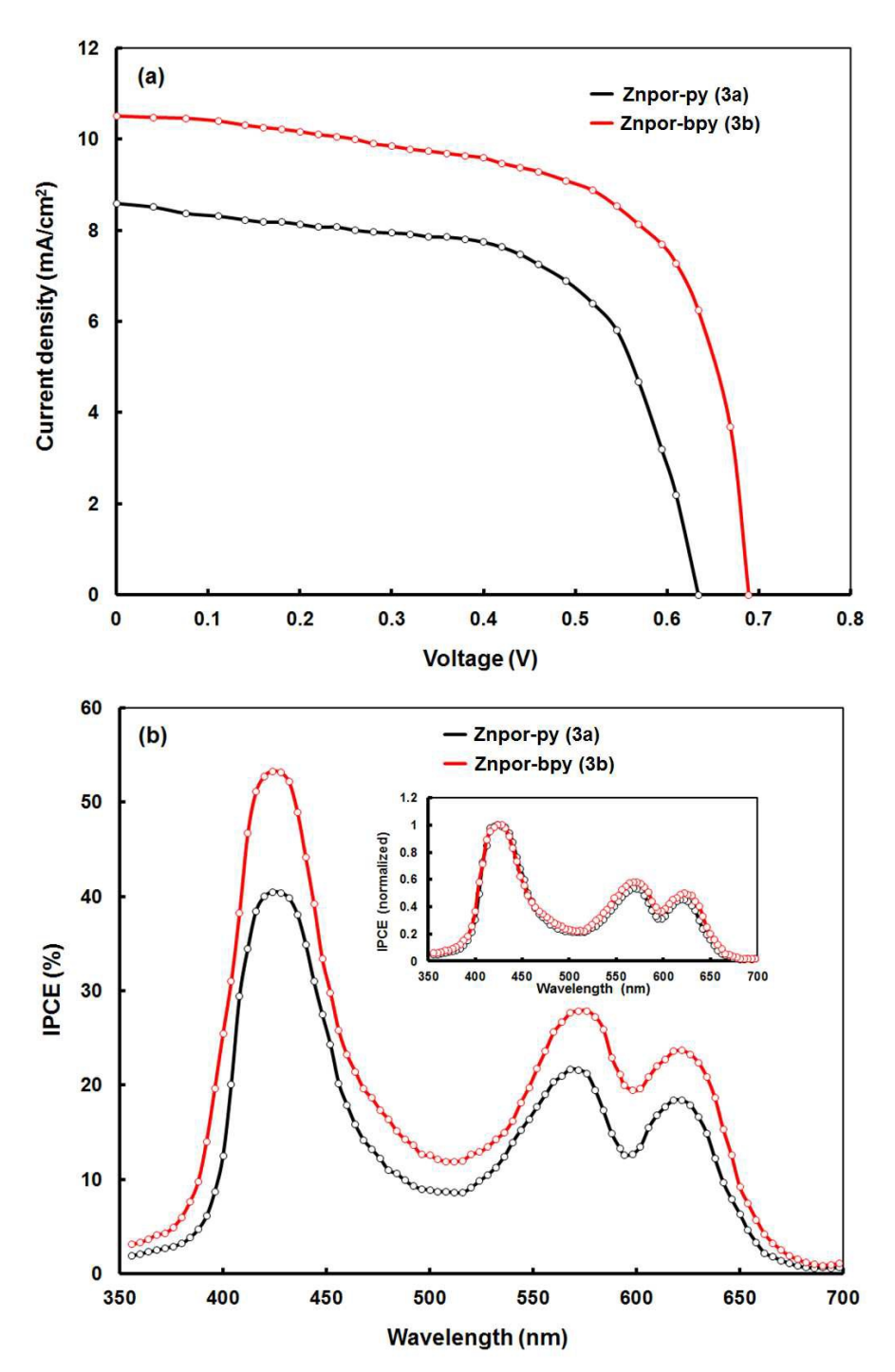


Figure 8. (a) Current-voltage (*J-V*) curves under illumination, and (b) IPCE spectra of DSSCs based on Znpor-py (3a) (black color) and Znpor-bpy (3b) (red color). The inset in IPCE spectra shows normalized IPCE responses at the wavelength region around the Soretand Q bands.

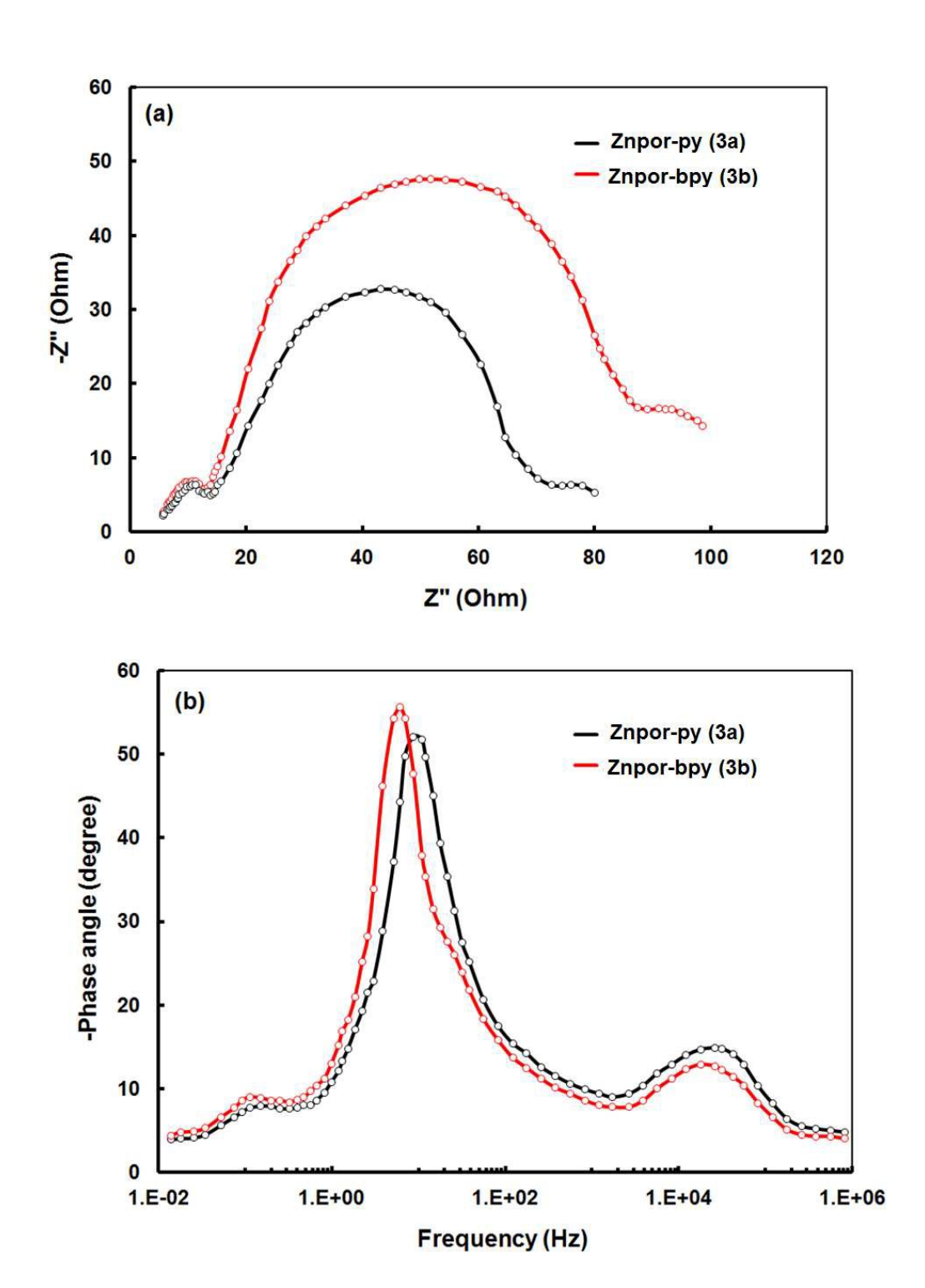
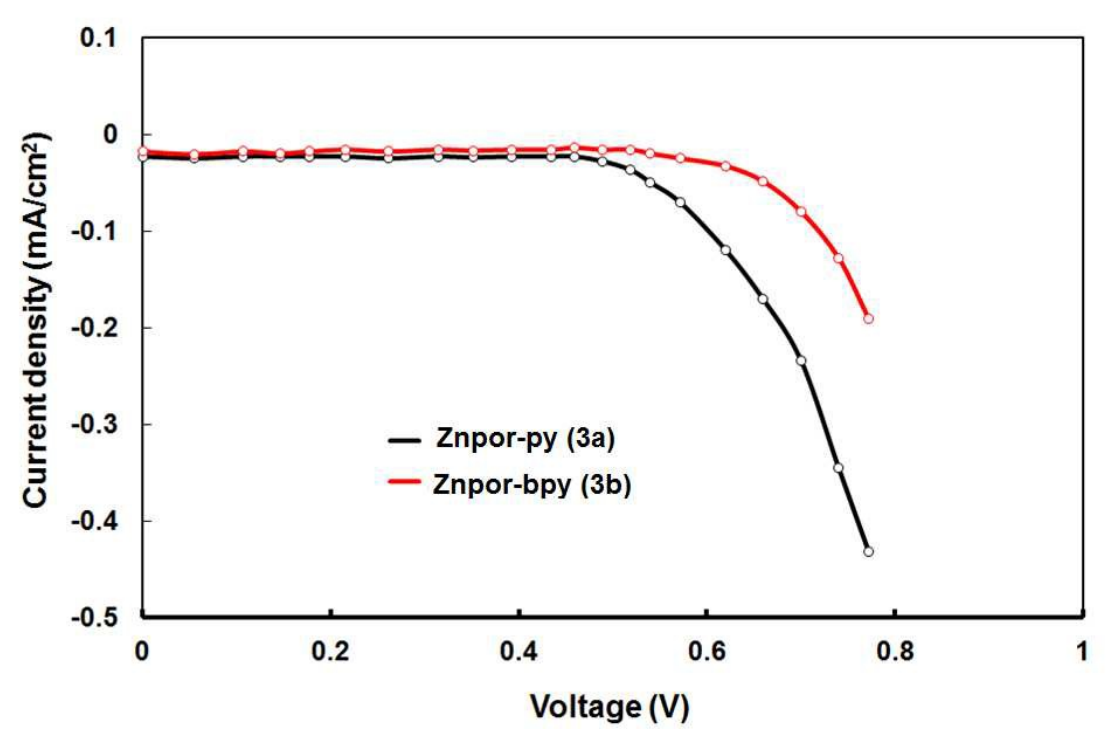


Figure 9. (a) Nyquist plots and (b) Bode phase plots of electrochemical impedance spectra of DSSCs sensitized with Znpor-py (3a) (black color) and Znpor-bpy (3b) (red color) in dark at open circuit condition.

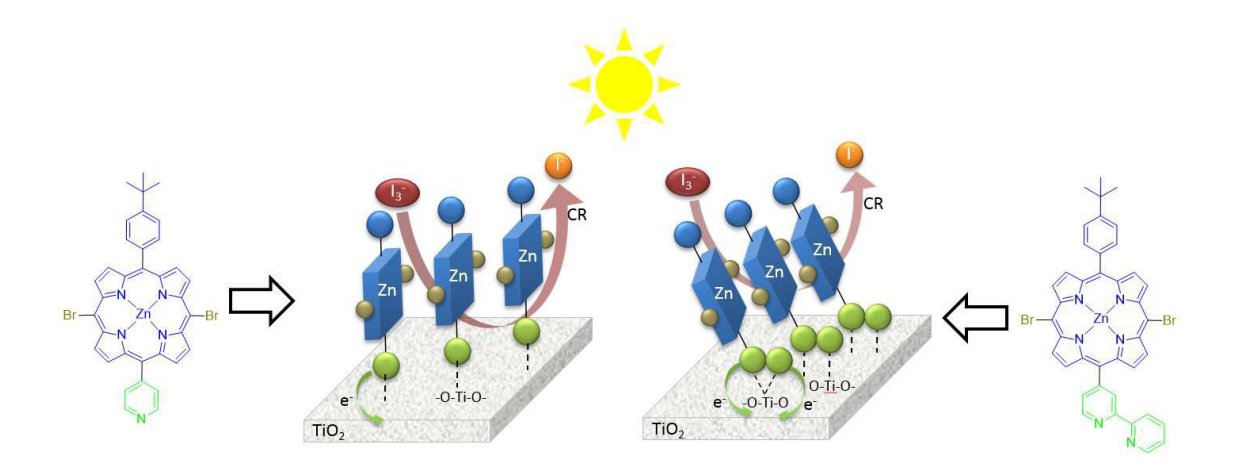


**Figure 10.** Current-voltage (*J-V*) curves in dark of DSSCs sensitized with Znpor-py (**3a**) (black color) and Znpor-bpy (**3b**) (red color).

For table of contents use only

## Pyridyl vs bipyridyl anchoring groups of porphyrin sensitizers for dye sensitized solar cells

Panagiotis A. Angaridis,  $^{\dagger}$ Eleftherios Ferentinos,  $^{\$}$ George Charalambidis,  $^{\$}$ Kalliopi Ladomenou,  $^{\$}$ Vasilis Nikolaou,  $^{\$}$ S. Biswas  $^{\$}$  Ganesh D. Sharma $^{*,\ddagger}$  and Athanassios G. Coutsolelos  $^{*,\$}$ 



## **Synopsis:**

Two D- $\pi$ -A porphyrins, which contain either pyridyl or bipyridyl electron acceptor-anchoring groups, are synthesized and used as sensitizers for the fabrication of dye-sensitized solar cells. The device sensitized by the bipyridyl-containing dye exhibits enhanced photovoltaic performance with respect to the one that is based on the pyridyl sensitizer. This is attributed to its faster electron injection into the TiO<sub>2</sub> photoanode and its reduced charge recombination at the electrode/electrolyte interface, which result from the stronger binding and coordination geometry of the bipyridine anchoring group on TiO<sub>2</sub>.

## References

- 1. B. Oregan and M. Gratzel, *Nature*, 1991, **353**, 737-740.
- 2. J. N. Clifford, E. Martinez-Ferrero, A. Viterisi and E. Palomares, *Chem. Soc. Rev.*, 2011, **40**, 1635-1646.
- 3. A. Hagfeldt, G. Boschloo, L. C. Sun, L. Kloo and H. Pettersson, *Chem. Rev.*, 2010, **110**, 6595-6663.
- 4. M. Gratzel, Acc. Chem. Res., 2009, 42, 1788-1798.
- 5. Z. J. Ning, Y. Fu and H. Tian, *Energ. Environal Sci.*, 2010, **3**, 1170-1181.
- 6. B. E. Hardin, H. J. Snaith and M. D. McGehee, *Nat. Photonics*, 2012, **6**, 162-169.
- 7. S. F. Zhang, X. D. Yang, Y. H. Numata and L. Y. Han, *Energ. Environal Sci.*, 2013, **6**, 1443-1464.
- 8. K. Kurotobi, Y. Toude, K. Kawamoto, Y. Fujimori, S. Ito, P. Chabera, V. Sundström and H. Imahori, *Chem. -Eur. J.*, 2013, **19**, 17075-17081.
- 9. K. Kakiage, Y. Aoyama, T. Yano, K. Oya, J.-i. Fujisawa and M. Hanaya, *Chem. Commun.*, 2015, **51**, 15894-15897.
- Z. Yao, M. Zhang, H. Wu, L. Yang, R. Li and P. Wang, J. Am. Chem. Soc., 2015, 137, 3799-3802.
- F. Gao, Y. Wang, D. Shi, J. Zhang, M. K. Wang, X. Y. Jing, R. Humphry-Baker, P. Wang, S. M. Zakeeruddin and M. Gratzel, *J. Am. Chem. Soc.*, 2008, 130, 10720-10728.
- 12. Q. J. Yu, Y. H. Wang, Z. H. Yi, N. N. Zu, J. Zhang, M. Zhang and P. Wang, *ACS Nano*, 2010, **4**, 6032-6038.
- 13. L. Y. Han, A. Islam, H. Chen, C. Malapaka, B. Chiranjeevi, S. F. Zhang, X. D. Yang and M. Yanagida, *Energ. Environal Sci.*, 2012, **5**, 6057-6060.
- 14. A. Mishra, M. K. R. Fischer and P. Bauerle, *Angew. Chem. Int. Edit.*, 2009, **48**, 2474-2499.
- 15. M. Liang and J. Chen, *Chem. Soc. Rev.*, 2013, **42**, 3453-3488.
- J. B. Yang, P. Ganesan, J. Teuscher, T. Moehl, Y. J. Kim, C. Y. Yi, P. Comte, K. Pei, T. W. Holcombe, M. K. Nazeeruddin, J. L. Hua, S. M. Zakeeruddin, H. Tian and M. Gratzel, J. Am. Chem. Soc., 2014, 136, 5722-5730.
- 17. W. H. Zhu, Y. Z. Wu, S. T. Wang, W. Q. Li, X. Li, J. A. Chen, Z. S. Wang and H. Tian, *Adv. Funct. Mater.*, 2011, **21**, 756-763.
- 18. W. D. Zeng, Y. M. Cao, Y. Bai, Y. H. Wang, Y. S. Shi, M. Zhang, F. F. Wang, C. Y. Pan and P. Wang, *Chem. Mater.*, 2010, **22**, 1915-1925.
- 19. M. Zhang, Y. L. Wang, M. F. Xu, W. T. Ma, R. Z. Li and P. Wang, *Energ. Environal Sci.*, 2013, **6**, 2944-2949.
- 20. H. Imahori, T. Umeyama and S. Ito, Acc. Chem. Res., 2009, 42, 1809-1818.
- 21. W. M. Campbell, A. K. Burrell, D. L. Officer and K. W. Jolley, *Coord. Chem. Rev.*, 2004, **248**, 1363-1379.
- 22. X. F. Wang and H. Tamiaki, *Energ. Environal Sci.*, 2010, **3**, 94-106.
- 23. M. K. Panda, K. Ladomenou and A. G. Coutsolelos, *Coord. Chem. Rev.*, 2012, **256**, 2601-2627.
- 24. G. E. Zervaki, V. Tsaka, A. Vatikioti, I. Georgakaki, V. Nikolaou, G. D. Sharma and A. G. Coutsolelos, *Dalton Trans.*, 2015, **44**, 13550-13564.
- 25. G. D. Sharma, G. E. Zervaki, K. Ladomenou, E. N. Koukaras, P. P. Angaridis and A. G. Coutsolelos, *J. Porphyrins Phthalocyanines*, 2015, **19**, 175-191.

- 26. V. Nikolaou, P. A. Angaridis, G. Charalambidis, G. D. Sharma and A. G. Coutsolelos, *Dalton Trans.*, 2015, 44, 1734-1747.
- 27. G. E. Zervaki, E. Papastamatakis, P. A. Angaridis, V. Nikolaou, M. Singh, R. Kurchania, T. N. Kitsopoulos, G. D. Sharma and A. G. Coutsolelos, *Eur. J. Inorg. Chem.*, 2014, **2014**, 1020-1033.
- 28. K. Ladomenou, T. N. Kitsopoulos, G. D. Sharma and A. G. Coutsolelos, *RSC Adv.*, 2014, **4**, 21379-21404.
- 29. P. A. Angaridis, T. Lazarides and A. C. Coutsolelos, *Polyhedron*, 2014, **82**, 19-32.
- 30. Z. E. Galateia, N. Agapi, N. Vasilis, G. D. Sharma and C. G. Athanassios, *J. Mater. Chem. C*, 2015, **3**, 5652-5664.
- 31. M. G. Walter, A. B. Rudine and C. C. Wamser, *J. Porphyrins Phthalocyanines*, 2010, **14**, 759-792.
- 32. L. L. Li and E. W. G. Diau, Chem. Soc. Rev., 2013, 42, 291-304.
- 33. T. Higashino and H. Imahori, *Dalton Trans.*, 2015, **44**, 448-463.
- 34. M. Urbani, M. Gratzel, M. K. Nazeeruddin and T. Torres, *Chem. Rev.*, 2014, **114**, 12330-12396.
- 35. L. Cabau, C. V. Kumar, A. Moncho, J. N. Clifford, N. Lopez and E. Palomares, *Energ. Environal Sci.*, 2015, **8**, 1368-1375.
- 36. J. Luo, M. F. Xu, R. Z. Li, K. W. Huang, C. Y. Jiang, Q. B. Qi, W. D. Zeng, J. Zhang, C. Y. Chi, P. Wang and J. S. Wu, *J. Am. Chem. Soc.*, 2014, **136**, 265-272.
- 37. C.-H. Wu, M.-C. Chen, P.-C. Su, H.-H. Kuo, C.-L. Wang, C.-Y. Lu, C.-H. Tsai, C.-C. Wu and C.-Y. Lin, *J. Mater. Chem. A*, 2014, **2**, 991-999.
- 38. A. Yella, H. W. Lee, H. N. Tsao, C. Y. Yi, A. K. Chandiran, M. K. Nazeeruddin, E. W. G. Diau, C. Y. Yeh, S. M. Zakeeruddin and M. Gratzel, *Science*, 2011, **334**, 629-634.
- 39. S. Mathew, A. Yella, P. Gao, R. Humphry-Baker, B. F. E. Curchod, N. Ashari-Astani, I. Tavernelli, U. Rothlisberger, M. K. Nazeeruddin and M. Gratzel, *Nature Chem.*, 2014, **6**, 242-247.
- 40. A. Yella, C. L. Mai, S. M. Zakeeruddin, S. N. Chang, C. H. Hsieh, C. Y. Yeh and M. Gratzel, *Angew. Chem. Int. Edit.*, 2014, **53**, 2973-2977.
- 41. C. Chen, X. C. Yang, M. Cheng, F. G. Zhang and L. C. Sun, *ChemSusChem*, 2013, **6**, 1270-1275.
- 42. B. Zietz, E. Gabrielsson, V. Johansson, A. M. El-Zohry, L. C. Sun and L. Kloo, *Phys. Chem. Chem. Phys.*, 2014, **16**, 2251-2255.
- 43. T. Higashino, Y. Fujimori, K. Sugiura, Y. Tsuji, S. Ito and H. Imahori, *Angew. Chem. Int. Ed.*, 2015, **54**, 9052-9056.
- 44. L. Zhang and J. M. Cole, *ACS Appl. Mater. Interfaces*, 2015, 7, 3427-3455.
- 45. Y. Ooyama, S. Inoue, T. Nagano, K. Kushimoto, J. Ohshita, I. Imae, K. Komaguchi and Y. Harima, *Angew. Chem. Int. Edit.*, 2011, **50**, 7429-7433.
- 46. Y. Ooyama, N. Yamaguchi, I. Imae, K. Komaguchi, J. Ohshita and Y. Harima, *Chem. Commun.*, 2013, **49**, 2548-2550.
- 47. Y. Ooyama, Y. Hagiwara, T. Mizumo, Y. Harima and J. Ohshita, *New J. Chem.*, 2013, **37**, 2479-2485.
- 48. Y. Ooyama, T. Nagano, S. Inoue, I. Imae, K. Komaguchi, J. Ohshita and Y. Harima, *Chem. -Eur. J.*, 2011, **17**, 14837-14843.
- 49. M. Cheng, X. C. Yang, J. J. Li, C. Chen, J. H. Zhao, Y. Wang and L. C. Sun, *Chem. Eur. J.*, 2012, **18**, 16196-16202.
- 50. J. F. Lu, X. B. Xu, Z. H. Li, K. Cao, J. Cui, Y. B. Zhang, Y. Shen, Y. Li, J. Zhu, S. Y. Dai, W. Chen, Y. B. Cheng and M. K. Wang, *Chem-Asian J*, 2013, **8**, 956-962.

- 51. C. L. Mai, T. Moehl, C. H. Hsieh, J. D. Decoppet, S. M. Zakeeruddin, M. Gratzel and C. Y. Yeh, *ACS Appl. Mater. Interfaces*, 2015, 7, 14975-14982.
- 52. D. Daphnomili, G. Landrou, S. P. Singh, A. Thomas, K. Yesudas, K. Bhanuprakash, G. D. Sharma and A. G. Coutsolelos, *RSC Adv.*, 2012, **2**, 12899-12908.
- 53. C. Stangel, A. Bagaki, P. A. Angaridis, G. Charalambidis, G. D. Sharma and A. G. Coutsolelos, *Inorg. Chem.*, 2014, **53**, 11871-11881.
- 54. J. K. Laha, S. Dhanalekshmi, M. Taniguchi, A. Ambroise and J. S. Lindsey, *Org. Process Res. Dev.*, 2003, 7, 799-812.
- 55. E. C. Constable, E. Figgemeier, C. E. Housecroft, J. Olsson and Y. C. Zimmermann, *Dalton Trans.*, 2004, 1918-1927.
- 56. B. Imperiali, T. J. Prins and S. L. Fisher, *J. Org. Chem.*, 1993, **58**, 1613-1616.
- 57. W. Kohn and L. J. Sham, *Phys. Rev.*, 1965, **140**, A1133-A1138.
- G. W. T. Gaussian 03; M. J. Frisch, H. B. Schlegel, G. E. Scuseria, M. A. Robb, J. R. Cheeseman, J. A. Montgomery, T. Vreven, K. N. Kudin, J. C. Burant, J. M. Millam, S. S. Lyengar, J. Tomasi, V. Barone, B. Mennucci, M. Cossi, G. Scalmani, N. Rega, G. A. Petersson, H. Nakatsuji, M. Hada, M. Ehara, K. Toyota, R. Fukuda, J. Hasegawa, M. Ishida, T. Nakajima, Y. Honda, O. Kitao, H. Nakai, M. Klene, X. Li, J. E. Knox, H. P. Hratchian, J. B. Cross, V. Bakken, C. Adamo, J. Jaramillo, R. Gomperts, R. E. Stratmann, O. Yazyev, A. J. Austin, R. Cammi, C. Pomelli, J. W. Ochterski, P. Y. Ayala, K. Morokuma, G. A. Voth, P. Salvador, J. J. Dannenberg, V. G. Zakrzewski, S. Dapprich, A. D. Daniels, M. C. Strain, O. Farkas, D. K. Malick, A. D. Rabuck, K. Raghavachari, J. B. Foresman, J. V. Ortiz, Q. Cui, A. G. Baboul, S. Clifford, J. Cioslowski, B. B. Stefanov, G. Liu, A. Liashenko, P. Piskorz, I. Komaromi, R. L. Martin, D. J. Fox, T. Keith, M. A. Al-Laham, C. Y. Peng, A. Nanayakkara, M. Challacombe, P. M. W. Gill, B. Johnson, W. Chen, M. W. Wong, C. Gonzalez, J. A. Pople, Gaussian 03, rev. D.01, Gaussian, Inc., Wallingford CT, 2004.
- 59. A. D. Becke, *Phys. Rev. A*, 1988, **38**, 3098-3100.
- 60. C. Lee, W. Yang and R. G. Parr, *Phys. Rev. B.*, 1988, **37**, 785-789.
- 61. D. A. Zhurko and G. A. Zhurko, *ChemCraft* 1.6, Plimus, San Diego, CA. Available at <a href="http://www.chemcraftprog.com">http://www.chemcraftprog.com</a>.
- 62. M. Cossi, V. Barone, R. Cammi and J. Tomasi, *Chem. Phys. Lett.*, 1996, **255**, 327-335.
- 63. J. Tomasi, B. Mennucci and R. Cammi, *Chem. Rev.*, 2005, **105**, 2999-3093.
- 64. G. D. Sharma, P. A. Angaridis, S. Pipou, G. E. Zervaki, V. Nikolaou, R. Misra and A. G. Coutsolelos, *Org. Electron.*, 2015, **25**, 295-307.
- 65. M. O. Senge, Chem. Commun., 2011, 47, 1943-1960.
- 66. B. S. Cheng and W. R. Scheidt, *Inorg. Chim. Acta*, 1995, **237**, 5-11.
- 67. W. R. Scheidt, K. M. Kadish, K. M. Smith and R. Guilard, Academic Press, 2000, 3.
- 68. K. Hara, M. Kurashige, Y. Dan-oh, C. Kasada, A. Shinpo, S. Suga, K. Sayama and H. Arakawa, *New J. Chem.*, 2003, **27**, 783-785.
- 69. J.-J. Kim, H. Choi, J.-W. Lee, M.-S. Kang, K. Song, S. O. Kang and J. Ko, *J. Mater. Chem.*, 2008, **18**, 5223-5229.
- 70. K. D. Seo, M. J. Lee, H. M. Song, H. S. Kang and H. K. Kim, *Dyes Pigm.*, 2012, **94**, 143-149.
- 71. F. Gou, X. Jiang, R. Fang, H. Jing and Z. Zhu, *ACS Appl. Mater. Interfaces*, 2014, **6**, 6697-6703.
- 72. B. K. An, S. K. Kwon, S. D. Jung and S. Y. Park, *J. Am. Chem. Soc.*, 2002, **124**, 14410-14415.
- 73. C. L. Wang, C. M. Lan, S. H. Hong, Y. F. Wang, T. Y. Pan, C. W. Chang, H. H. Kuo, M. Y. Kuo, E. W. G. Diau and C. Y. Lin, *Energ. Environal Sci.*, 2012, **5**, 6933-6940.

- 74. M. Gouterman, J. Mol. Spectrosc., 1961, **6**, 138-163.
- 75. Y. Ooyama, S. Inoue, T. Nagano, K. Kushimoto, J. Ohshita, I. Imae, K. Komaguchi and Y. Harima, *Angew. Chem. Int. Ed.*, 2011, **50**, 7429-7433.
- 76. M. K. Nazeeruddin, A. Kay, I. Rodicio, R. Humphrybaker, E. Muller, P. Liska, N. Vlachopoulos and M. Gratzel, *J. Am. Chem. Soc.*, 1993, **115**, 6382-6390.
- 77. T. Marinado, K. Nonomura, J. Nissfolk, M. K. Karlsson, D. P. Hagberg, L. C. Sun, S. Mori and A. Hagfeldt, *Langmuir*, 2010, **26**, 2592-2598.
- 78. M. Adachi, M. Sakamoto, J. T. Jiu, Y. Ogata and S. Isoda, *J. Phys. Chem. B*, 2006, **110**, 13872-13880.
- 79. F. Fabregat-Santiago, J. Bisquert, E. Palomares, L. Otero, D. B. Kuang, S. M. Zakeeruddin and M. Gratzel, *J. Phys. Chem. C*, 2007, **111**, 6550-6560.